Intrinsic plasticity of cerebellar stellate cells is mediated by NMDA receptor regulation of voltage-gated Na$^+$ channels

Ryan P.D. Alexander[1,2] and Derek Bowie[2]

[1]*Integrated Program in Neuroscience, McGill University, Montréal, Québec, Canada*
[2]*Department of Pharmacology and Therapeutics, McGill University, Montréal, Québec, Canada*

Edited by: Katalin Toth & Jean-Claude Béïque

The Journal of Physiology

Key points

- We show that NMDA receptors (NMDARs) elicit a long-term increase in the firing rates of inhibitory stellate cells of the cerebellum
- NMDARs induce intrinsic plasticity through a Ca^{2+}- and CaMKII-dependent pathway that drives shifts in the activation and inactivation properties of voltage-gated Na$^+$ (Na$_v$) channels
- An identical Ca^{2+}- and CaMKII-dependent signalling pathway is triggered during whole-cell recording which lowers the action potential threshold by causing a hyperpolarizing shift in the gating properties of Na$_v$ channels.
- Our findings open the more general possibility that NMDAR-mediated intrinsic plasticity found in other cerebellar neurons may involve similar shifts in Na$_v$ channel gating.

Abstract   Memory storage in the mammalian brain is mediated not only by long-lasting changes in the efficacy of neurotransmitter receptors but also by long-term modifications to the activity of voltage-gated ion channels. Activity-dependent plasticity of voltage-gated ion channels, or intrinsic plasticity, is found throughout the brain in virtually all neuronal types, including principal cells and interneurons. Although intrinsic plasticity has been identified in neurons of the cerebellum, it has yet to be studied in inhibitory cerebellar stellate cells of the molecular layer which regulate activity outflow from the cerebellar cortex by feedforward inhibition onto Purkinje cells. The study of intrinsic plasticity in stellate cells has been particularly challenging as membrane patch breakthrough in electrophysiology experiments unintentionally triggers changes in spontaneous firing rates. Using cell-attached patch recordings to avoid disruption, we show that activation of extrasynaptic *N*-methyl-D-aspartate receptors (NMDARs) elicits a long-term increase in the firing properties of stellate cells by stimulating a rise in cytosolic Ca^{2+} and activation of Ca^{2+}/calmodulin-dependent protein kinase II (CaMKII). An identical signalling pathway is triggered during whole-cell recording which lowers the action potential threshold by causing a hyperpolarizing shift in the gating properties of voltage-gated sodium (Na$_v$) channels. Together, our findings identify an unappreciated role of Na$_v$ channel-dependent intrinsic plasticity in cerebellar stellate cells which, in concert with

---

Ryan Alexander earned a BSc at the University of Alberta in his hometown of Edmonton, Canada, in 2010. He then travelled to Munich, Germany, to obtain a MSc Neuroscience at the Ludwig-Maximilians-Universität under the supervision of Drs Jana Hartmann and Arthur Konnerth. He returned to Canada in 2013 to begin a PhD at McGill University in Montréal, QC, with Dr Derek Bowie. An enthusiasm for cerebellar synaptic signalling originating in Munich was further honed in Montréal where he developed a distinct interest in long-term, activity-dependent modulation of voltage-gated Na$^+$ channels in molecular layer interneurons.

---

non-canonical NMDAR signalling, provides the cerebellum with an unconventional mechanism to fine-tune motor behaviour.

Corresponding author Dr D. Bowie: Department of Pharmacology & Therapeutics, McGill University, Bellini Life Sciences Building, Room 164, 3649 Promenade Sir William Osler, Montréal, Québec, Canada, H3G 0B1. Email: derek.bowie@mcgill.ca

Introduction

N-Methyl-D-aspartate receptors (NMDARs) are members of the ionotropic glutamate receptor family of ion channels that mediate most fast excitatory synaptic transmission in the developing and mature CNS (Dingledine *et al.* 1999; Traynelis *et al.* 2010). They are essential for life and have primary roles in neuronal development (Constantine-Paton *et al.* 1990), learning and memory (Madison *et al.* 1991) as well as being strongly implicated in neurological disease (Hardingham & Bading, 2010; Paoletti *et al.* 2013; Myers *et al.* 2019). The ion channel pore of the NMDAR is exquisitely structured to permit the rapid transport of external Ca^{2+} when the neuron is depolarized (Huettner, 2015). At resting membrane potentials, it is tonically blocked by external Mg^{2+} ions (Dingledine *et al.* 1999), which act as a gatekeeper to ensure that NMDARs pass only pertinent information to the postsynaptic cell. The rise in cytosolic Ca^{2+} that follows NMDAR activation triggers several intracellular signalling pathways that either promote neuronal health or are detrimental to it. Synaptic GluN2A-containing NMDARs are most notably associated with the activation of Ca^{2+}/calmodulin-dependent protein kinase II (CaMKII) by the Ca^{2+}–calmodulin complex (De Koninck & Schulman, 1998), which drives a number of post-synaptic processes including the synaptic recruitment of AMPA receptors (AMPARs) and long-term potentiation (LTP) (Herring & Nicoll, 2016). In contrast, Ca^{2+} transport through extrasynaptic GluN2B-containing NMDARs is associated with the activation of neuronal nitric oxide synthase and other signalling molecules that promote cell death (Hardingham & Bading, 2010).

This canonical view of GluN2A- and GluN2B-containing NMDARs has evolved recently with the appreciation of greater subunit diversity including the formation of tri-heteromers which offer additional functionality (Paoletti *et al.* 2013; Hansen *et al.* 2018). In inhibitory stellate cells (SCs) of the cerebellum, for example, glutamatergic synapses are apparently devoid of NMDARs but possess extrasynaptic receptors that are activated under conditions such as high frequency stimulation of presynaptic fibres, which promote neurotransmitter spillover (Carter & Regehr, 2000; Clark & Cull-Candy, 2002; Szapiro & Barbour, 2007; Coddington *et al.* 2013). Genetic deletion and pharmacology experiments suggest that SCs express tri-heteromeric

NMDARs containing both GluN2B and 2D receptor subunits (Dubois *et al.* 2016) that promote long-lasting GABA release either directly (Liu & Lachamp, 2006; Liu, 2007) through a protein kinase A (PKA) pathway (Lachamp *et al.* 2009), or indirectly via axonal Ca^{2+} channels (Christie & Jahr, 2008). Stimulation of extrasynaptic NMDARs also alters the composition of synaptic AMPARs via a protein kinase C (PKC)-dependent pathway (Liu *et al.* 2008). Although Ca^{2+} entry through extrasynaptic NMDARs of SCs has recently been shown to activate nNOS (Larson *et al.* 2020), the possible signalling role of CaMKII has yet to be explored.

Here, we identify a novel role for extrasynaptic NMDARs which elicit a long-term increase in the intrinsic firing properties of cerebellar SCs by targeting voltage-gated sodium (Na_v) channels. Upregulation in intrinsic excitability is mediated by cytosolic Ca^{2+} and CaMKII which target Na_v channels causing a hyper-polarizing shift in their activation and inactivation gating behaviour to favour action potential (AP) firing. Given that SCs regulate the firing properties of Purkinje cells through feedforward inhibition, our findings identify a novel mechanism by which NMDARs regulate information outflow from the cerebellar cortex.

Methods

Ethical approval

All experiments were performed in accordance with the guidelines of the Canadian Council on Animal Care and were approved by the Animal Care Committee of McGill University (approval #2013-7435).

Animals

Wild-type mice with a C57BL/6J background were obtained from Charles River Laboratories (Wilmington, MA, USA) and maintained as a breeding colony at McGill University. Both male and female wild-type mice used for the experiments ranged from postnatal days 18 to 30. Animals were permitted *ad libitum* access to food and water.

Slice preparation

Mice were anaesthetized with isoflurane and immediately decapitated. A block of cerebellar vermis was rapidly

dissected from the mouse head and submerged in ice-cold cutting solution perfused with carbogen gas (95% O_2, 5% CO_2). Cutting solution contains (in mM): 235 sucrose, 2.5 KCl, 1.25 NaH_2PO_4, 28 $NaHCO_3$, 0.5 $CaCl_2$, 7 $MgCl_2$, 28 D-glucose, 1 ascorbic acid, 3 sodium pyruvate (pH 7.4; 305−315 mOsmol l^{-1}). The block of vermis was then fastened to a platform, transferred to the slicing chamber and again submerged in ice-cold cutting solution bubbled with carbogen throughout the remainder of the procedure. Thin slices of cerebellar vermis (300 μm) were obtained with a vibrating tissue sectioner (Leica VT1200; Leica Instruments, Nussloch, Germany). The slices were transferred to oxygenated artificial cerebrospinal fluid (ACSF) and held at room temperature (21°C–23°C) for at least 1 h before recordings were performed. ACSF contained the following (in mM): 125 NaCl, 2.5 KCl, 1.25 NaH_2PO_4, 26 $NaHCO_3$, 2 $CaCl_2$, 1 $MgCl_2$, 25 D-glucose (pH of 7.4; 305−315 mOsmol l^{-1}).

Electrophysiology

Slice experiments were performed on an Olympus BX51 upright microscope (Olympus, Southall, UK) equipped with differential interference contrast/infrared optics. Whole-cell patch-clamp recordings were made from visually identified SCs in acute sagittal slices of cerebellar vermis. SCs were distinguished from misplaced or migrating granule, glial or basket cells by their small soma diameter (8−9 μm), location in the outer two-thirds of the molecular layer and whole-cell capacitance measurement (4−12 pF). Patch pipettes were prepared from thick-walled borosilicate glass (GC150F-10, OD 1.5 mm, ID 0.86 mm; Harvard Apparatus Ltd, Kent, UK) with open tip resistances of 4−7 MΩ when filled with an intracellular recording solution. Recordings were made with a Multiclamp 700A amplifier (Molecular Devices, Sunnyvale, CA, USA) at a holding potential of −70 mV. Series resistance and whole-cell capacitance were estimated by cancelling the fast transients evoked at the onset and offset of brief (10 ms) 5 mV voltage-command steps. Access resistance during whole-cell recording (7−25 MΩ) was compensated between 60 and 80% and checked for stability throughout the experiments (∼15% tolerance). The bath was continuously perfused at room temperature (21−23°C) with ACSF at a rate of 1−2 ml min^{-1}. Currents were filtered at 5 kHz with an eight-pole low-pass Bessel filter (Frequency Devices, Haverhill, MA, USA) and digitized at either 25 or 100 kHz with a Digidata 1322A data acquisition board and Clampex 10.1 (Molecular Devices) software. For voltage-clamp recordings, the online P/N leak-subtraction suite in Clampex 10.1 was used to assess voltage-gated responses, and raw current traces were collected simultaneously.

For recording voltage-dependence of activation of I_A, a protocol was applied consisting of 500 ms steps evoked from a holding potential of −100 mV, ranging from −100 mV to +20 mV in 10 mV increments. An inactivation protocol was applied consisting of 500 ms prepulse steps ranging from −120 mV to −30 mV in 5 mV increments, followed by a probe step to −20 mV to assess voltage-dependence of steady-state inactivation, or channel availability. Due to space clamp issues, it is not possible to record the fast gating of sodium current in SCs with conventional voltage-clamp protocols. The main problem is the inability to accurately record sodium channel activity in distant processes such as axons. To circumvent this, we adapted a protocol by using a depolarizing prepulse step to inactivate sodium channels distant from the recording electrode which was followed shortly afterwards with a second test step to record sodium channels close to the cell soma (Milescu *et al.* 2010). This consisted of a suprathreshold step from −80 mV to −35 mV in order to evoke an action current, followed by a ∼1 ms step to −60 mV, followed by steps ranging from −80 mV to +30 mV in 5 mV increments. To measure steady-state inactivation, we employed a protocol consisting of 100 ms steps ranging from −110 mV to −20 mV in 5 mV increments, followed by a probe step to −20 mV.

Perforated-patch recordings were obtained in the same external ACSF described above. Amphotericin B powder was dissolved in DMSO on the day of the experiment at a concentration of 60 mg ml^{-1}. This stock solution was added to an aliquot of internal pipette solution at a concentration of 300 μg ml^{-1}. Borosilicate patch electrodes (4−6 MΩ) were first dipped in an antibiotic-free internal solution for a few seconds, followed by back-filling with the amphotericin B-containing internal solution. The internal pipette solution was also supplemented with 1 mM Lucifer Yellow to verify the integrity of the plasma membrane post-recording.

For parallel fibre (PF) stimulation experiments, pipettes were pulled using thin-walled borosilicate glass (OD 1.65 mm, ID 1.15 mm; King Precision Glass Inc., Claremont, CA, USA) exhibiting 1−2 MΩ tip resistance when filled with ACSF. Voltage pulses (10−25 V in amplitude, 200−400 μs in duration) were applied through the stimulating electrode positioned in the molecular layer just beneath the surface of the slice. To minimize variability between responses, the stimulating electrode was positioned 50−100 μm away from the recorded cell. Stimulation strength and duration were kept constant throughout the experiment. For high frequency stimulation, trains of six stimuli were delivered at 100 Hz (inter-train interval of 10 s), which mimics sensory activation patterns of granule cells *in vivo* (Jorntell & Ekerot, 2006; Saviane & Silver, 2006; Rancz *et al.* 2007) and has been demonstrated to activate the

extrasynaptically located NMDARs in molecular layer interneurons (Carter & Regehr, 2000; Clark & Cull-Candy, 2002).

Recording solutions

All chemicals were obtained from Sigma Aldrich (St. Louis, MO, USA) unless otherwise indicated. The internal pipette solution for most current-clamp experiments contained (in mM): 126 K-gluconate, 5 Hepes, 4 NaCl, 15 D-glucose, 0.05 $CaCl_2$, 1 $MgSO_4$, 0.15 K_4-BAPTA, 3 Mg-ATP, 0.1 Na-GTP (adjusted to pH 7.4 with KOH, 300–310 mOsmol l^{-1}). For current-clamp experiments with high internal BAPTA, K_4-BAPTA was increased to 10 mM and K-gluconate reduced to 110 mM. The pipette solution for voltage-clamp experiments examining A-type K^+ current (I_A) contained (in mM): 140 KCl, 10 Hepes, 2.5 $MgCl_2$, 0.15 K_4-BAPTA (adjusted to pH 7.4 with KOH, 300–310 mOsmol l^{-1}). For these experiments the external ACSF was supplemented with 5 mM TEA-Cl and 2 mM CsCl to block non-I_A-mediating K^+ channels, and 100 nM TTX to block firing. The pipette solution for voltage-clamp experiments examining transient Na^+ current (I_{Na}) contained (in mM): 110 Cs-methanosulfate, 5 Hepes, 4 NaCl, 15 D-glucose, 0.05 $CaCl_2$, 0.15 Cs_4-BAPTA, 4 Mg-ATP, 0.1 Na-GTP, 10 TEA-Cl, 10 4-AP (adjusted to pH 7.4 with CsOH, 300–310 mOsmol l^{-1}). For the experiments isolating I_{Na}, the external ACSF was supplemented with 100 μM $CdCl_2$ and 1 μM Mibefradil dihydrochloride (Tocris Bioscience, Ellisville, MO, USA) to block voltage-gated calcium channels. BAPTA-AM (Abcam, Cambridge, UK) was used to incubate slices in a membrane-permeable Ca^{2+} chelator. Free Ca^{2+} concentration for control low BAPTA internal solutions was calculated to be ∼100 nM using MaxChelator freeware (Bers *et al.* 2010), which is the expected physiological level for neurons. For cell-attached experiments, the internal solution contained (in mM): 125 NaCl, 10 Hepes, 40 D-glucose, 2.5 $MgCl_2$ (adjusted to pH 7.4 with NaOH, 300–310 mOsmol l^{-1}). Except where indicated, all experiments were performed in the presence of fast excitatory and inhibitory synaptic blockers: NMDA receptor antagonist D-(-)-2-Amino-5 phosphonopentanoic acid (D-APV; 10 μM), AMPA/kainate receptor antagonist 2,3-Dioxo-6-nitro-1,2,3,4-tetrahydrobenzo[f]quinoxaline-7-sulfonamide (NBQX; 10 μM) and GABA-A receptor antagonist bicuculline (BIC; 10 μM) were purchased from Abcam (Cambridge, UK).

Data analysis and statistics

Voltage-dependence of activation for all current types was analysed by first calculating conductance (G) values from the peak currents elicited by each respective activation protocol using the formula:

$$G_x = \frac{I_x}{V_m - V_{rev_x}}$$

where I_x is the peak current of current type x (i.e. I_A, I_{Na}) evoked at membrane potential V_m, and V_{rev_x} is the reversal potential of current type x. Conductance–voltage relationships for each current type were then fit to a Boltzmann function using the formula:

$$G_x = \frac{G_{max}}{(1 + \exp((V_{1/2} - V_m)/k))}$$

where G_x is the conductance at membrane potential V_m for current type x, G_{max} is the maximum conductance for current type x, $V_{1/2}$ is the membrane potential where G_x is 50% of G_{max}, and k is the slope factor. Boltzmann fits were performed for each time point in each cell in order to calculate normalized conductance values. Summary conductance–voltage relationships for each current type were calculated by averaging the normalized conductance values across all cells in the dataset. $V_{1/2}$ values reported in the *Results* section for each current type were calculated by fitting the normalized conductance averages.

Paired *t* tests were used to compare electrophysiological data recorded at baseline and after 25 min (step-evoked AP frequency, AP threshold, $V_{1/2}$ values for I_{Na} and I_A, spontaneous firing rate). Unpaired *t* tests and one-way ANOVA (with *post hoc* decomposition using Fisher's least significant difference (LSD) method) were used in some instances to compare electrophysiological data between controls and different pharmacological conditions (baseline AP threshold, baseline $V_{1/2}$ activation and inactivation values, $\Delta V_{1/2}$ values, baseline spontaneous action current frequencies). F-ratio tests were used to examine differences in Boltzmann fits of conductance–voltage data of sodium currents, which compares the k as well as $V_{1/2}$ fit parameters. For each experimental group, recordings from a minimum of five cells from a minimum of three animals were collected. Analysis was not blinded.

Data are reported as means ± 95% confidence interval. Significance was denoted with $^*P < 0.05$ and $^{**}P < 0.01$. All fitting was performed with Origin 7.0. Statistical analyses were performed using SPSS 17.0 and GraphPad Prism 8.

Results

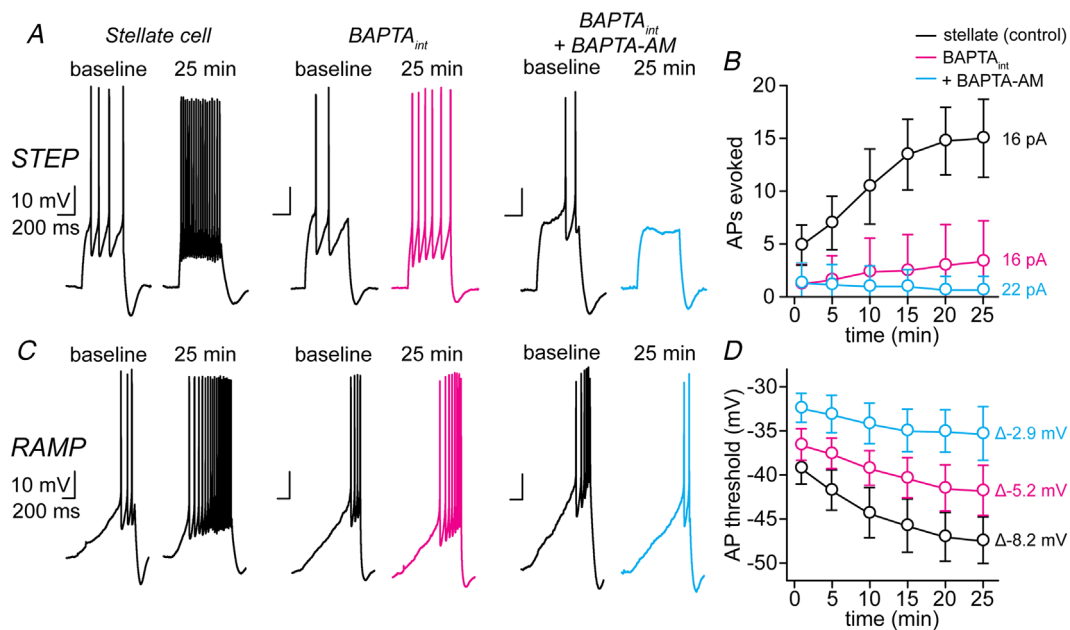### Action potential threshold is regulated by intracellular Ca^{2+} in cerebellar stellate cells

Cerebellar SCs undergo a time-dependent increase in the rate of AP firing following patch breakthrough to establish

whole-cell recording (Alexander *et al.* 2019). Although the underlying mechanism is still unresolved, our previous work using Hodgkin–Huxley modelling suggests that increased AP firing is primarily due to a hyperpolarizing shift in both the activation and inactivation properties of Na_v channels (Alexander *et al.* 2019). Since other studies have suggested that increased neuronal excitability might be linked to elevations in cytosolic Ca^{2+} (Gall *et al.* 2003; Alcami *et al.* 2012), we tested whether it could be attenuated or eliminated by Ca^{2+} chelation with BAPTA.

In keeping with this, inclusion of 10 mM BAPTA in the internal recording solution significantly attenuated AP firing in SCs following whole-cell recording (Fig. 1*A* and *B*). The number of APs evoked by a 16 pA depolarizing step in control conditions (4.9 ± 2.8 at baseline *vs.* 15.0 ± 5.5 at 25 min; $t = 4.73$, $P < 0.001$; $n = 11$) was attenuated about fourfold in recordings with 10 mM internal BAPTA (1.3 ± 2.0 at baseline *vs.* 3.4 ± 3.8 at 25 min; $t = 1.86$, $P = 0.11$; $n = 8$) after 25 min of recording (Fig. 1*A* and *B*). More strikingly, the increase in firing rate was completely eliminated in slices pre-incubated with BAPTA-AM (150 μM) such that the number of APs observed following step depolarizations of 22 pA was the same at the start of the experiment and after 25 min (1.1 ± 1.7 at baseline *vs.* 0.6 ± 1.1 at 25 min; $t = 1.58$,

$P = 0.17$; $n = 6$) (Fig. 1*A* and *B*). Although 10 mM internal BAPTA would lower resting Ca^{2+} below physiological levels, the fact that the increase in SC excitability is eliminated only after pre-incubation with BAPTA-AM suggests that Ca^{2+} acts on a rapid time scale since its chelation must be in place in advance of patch breakthrough. Taken together, these observations demonstrate that the formation of whole-cell recording augments SC excitability by elevating cytosolic Ca^{2+}.

To establish a causal link between the rise in cytosolic Ca^{2+} to shifts in Na_v channel gating, we performed current ramp experiments to measure the membrane potential at which APs are initiated (i.e. AP threshold) (Fig. 1*C* and *D*). Our previous work using Hodgkin–Huxley modelling accounted for the shifts in AP threshold by the hyperpolarizing shifts in Na_v channel gating (Alexander *et al.* 2019). In control conditions, the AP threshold hyperpolarized by 8.3 ± 1.1 mV over 25 min of recording (-39.7 ± 1.8 mV at baseline *vs.* -48.1 ± 2.5 mV at 25 min; $t = 15.74$, $P < 0.001$; $n = 12$) (Fig. 1*C* and *D*), which was attenuated by 10 mM internal BAPTA, hyperpolarizing by 5.2 ± 2.8 mV (-36.5 ± 1.7 mV at baseline *vs.* -41.7 ± 2.7 mV at 25 min; $t = 3.53$, $P = 0.012$; $n = 8$). The attenuation in the shift in AP threshold was even more substantial compared with control conditions following pre-incubation with

Figure 1. Cerebellar stellate cell excitability depends on intracellular Ca^{2+}
A, step-evoked AP firing in example stellate cells (SCs) at baseline and after 25 min of whole-cell patch-clamp recording in control (patch # 150129p2), 10 mM internal BAPTA (patch # 181106p4), and following >1 h incubation in 150 μM BAPTA-AM (patch # 181030p4). *B*, time course plot of averaged AP frequency evoked by one example step amplitude for control ($n = 12$ cells), 10 mM BAPTA internal ($n = 8$ cells) and 150 μM BAPTA-AM incubation conditions ($n = 6$ cells). *C*, example current-clamp responses evoked by a ramp protocol at baseline and after 25 min in SCs. *D*, summary plot depicting change in AP threshold over time in SCs in control and BAPTA conditions. Δ mV measurements denote the change in AP threshold from baseline to 25 min later. Data are depicted as means $\pm$ SD.

BAPTA-AM ($t = 6.66$, $P < 0.001$), hyperpolarizing by only 2.9 ± 1.7 mV (-32.4 ± 1.1 mV at baseline *vs.* -35.3 ± 2.2 mV at 25 min; $t = 3.38$, $P = 0.015$; $n = 7$) (Fig. 1*C* and *D*). These observations, particularly with BAPTA-AM, establish a causal relationship between a rise in cytoplasmic Ca^{2+} and the hyperpolarizing shift in AP threshold.

Taken together, these findings demonstrate the importance of intracellular Ca^{2+} in initiating the increase in membrane excitability of SCs following patch break-through and the potential role of Na_v channels. Since Ca^{2+} often mediates its effects on ion channels, including Na_v channels, through kinase activity (Levitan, 1994), we next performed experiments to determine the role of signalling by phosphorylation and to identify which kinase(s) may be involved.

CaMKII, but not PKC, promotes an increase in stellate cell excitability

The potential role of protein kinases on AP threshold was studied first using the broad-spectrum kinase inhibitor, staurosporine (2μM) (Fig. 2*A* and *B*). To ensure complete inhibition of all kinase activity, cerebellar slices were pre-incubated with staurosporine before the start of the experiment and then included in the internal and external recording solutions to maintain pharmacological block. Under these conditions, the increase in SC excitability observed in control cells was eliminated by staurosporine. For example, during a 16 pA depolarizing step, APs evoked at the beginning of the experiment and after 25 min of recording were similar in slices treated with staurosporine (4.0 ± 2.9 at baseline *vs.* 4.7 ± 4.1 at 25 min; $t = 1.22$, $P = 0.27$; $n = 7$). Similarly, staurosporine significantly attenuated the shift in AP threshold and thus implicated a role for Na_v channel gating. In the presence of staurosporine, the AP threshold hyperpolarized about twofold less than the control ($\Delta -3.7 \pm 1.4$ mV for staurosporine *vs.* $\Delta -8.3 \pm 1.1$ mV for control; $t = 5.40$, $P < 0.001$; staurosporine: $n = 7$ cells, control: $n = 12$ cells) (Fig. 2*A* and *B*). These observations implicate cytoplasmic kinases in regulating SC excitability, most likely by regulating Na_v channel gating.

To elucidate which kinases might be involved, we chose inhibitors of two commonly occurring kinases known to be involved in Ca^{2+} signalling which include Gö 6983 (1μM) for protein kinase C (PKC) (Bouhours *et al.* 2011), and both KN93 (5μM) and Autocamtide-2-related inhibitory peptide (AIP; 1μM) for Ca^{2+}/calmodulin-dependent protein kinase II
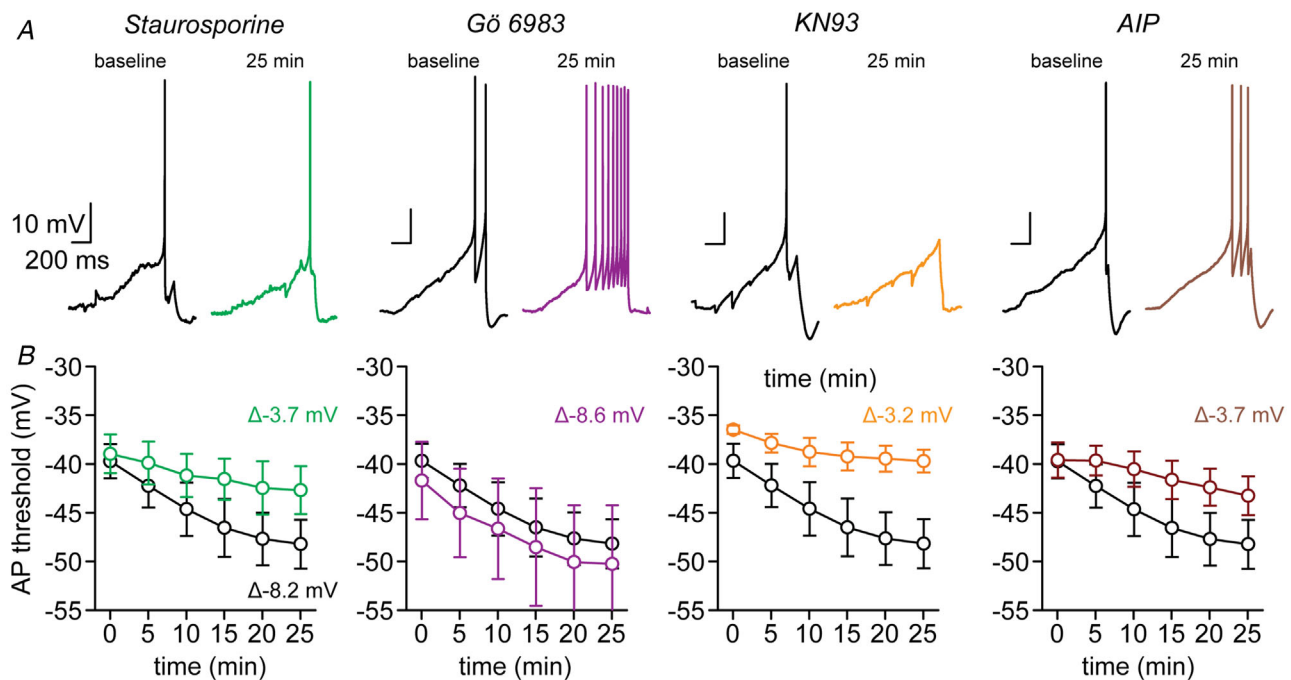

Figure 2. CaMKII, but not PKC, regulates excitability in stellate cells
A, current-clamp traces from example stellate cells (SCs) in the presence of various protein kinase inhibitors, including staurosporine (patch # 150402p4), Gö 6983 (patch # 150420p4), KN93 (patch # 150521p3) and AIP (patch # 201001p4). In each case, the left trace is immediately following patch breakthrough and the right trace is 25 min later. *B*, summary time course plots depicting AP threshold change in the presence of each kinase inhibitor compared with control (control, $n = 12$ cells; staurosporine, $n = 7$ cells; Gö 6983, $n = 5$ cells; KN93, $n = 6$ cells; AIP, $n = 7$ cells). Δ mV measurements denote the change in AP threshold from baseline to 25 min later. Data are depicted as means $\pm$ SD.

(CaMKII) (Fig. 2*A* and *B*). As before, cerebellar slices were pre-incubated with each inhibitor before the start of the experiment and included in the internal and external recording solutions. Using this approach, we eliminated the increase in SC excitability by blocking CaMKII but not PKC activity. For example, a pharmacological block of PKC with Gö 6983 did not affect the increase in SC excitability following patch breakthrough, where the number of APs evoked at the beginning of the experiment and after 25 min of recording increased significantly (0.4 ± 0.5 at baseline *vs.* 10.0 ± 5.5 at 25 min; $t = 3.24$, $P = 0.032$; $n = 5$). Similarly, a pharmacological block of PKC yielded little difference in the hyperpolarizing shift observed in AP threshold relative to control cells ($\Delta -8.6 \pm 2.9$ mV for Gö 6983 *vs.* $\Delta -8.3 \pm 1.1$ mV for control; $t = 0.05$, $P = 0.96$; Gö 6983: $n = 5$ cells, control: $n = 12$ cells) (Fig. 2*A* and *B*). In contrast, APs evoked by a 16 pA step at the beginning of the experiment and after 25 min of recording were similar in slices where CaMKII activity was blocked with KN93 (0.8 ± 1.1 at baseline *vs.* 0.2 ± 0.3 at 25 min; $t = 1.54$, $P = 0.19$; $n = 6$) or AIP (0.3 ± 0.6 at baseline *vs.* 1.4 ± 1.5 at 25 min; $t = 2.07$, $P = 0.084$; $n = 7$). Moreover, the shift in AP threshold was significantly attenuated, hyperpolarizing by only 3.2 ± 0.8 mV with KN93 and 3.7 ± 1.5 mV with AIP, compared with 8.3 ± 1.1 mV for control (KN93: $t = 6.70$, $P < 0.001$; $n = 6$; AIP: $t = 5.33$, $P < 0.001$; $n = 7$) (Fig. 2*A* and *B*).

These data implicate the rise in cytosolic Ca^{2+} elicited by whole-cell patch breakthrough to the activation of CaMKII. The fact that a pharmacological block of this kinase also greatly attenuated the hyperpolarizing shift in AP threshold suggests that CaMKII may directly or indirectly modulate the gating properties of Na_v channels expressed by cerebellar SCs. Given this, we next tested the effect of Ca^{2+} chelation and kinase inhibition on isolated Na_v channel currents measured in voltage-clamp recordings (Figs 3 and 4). We also tested these conditions on isolated A-type K^+ currents (Fig. 5). Although A-type K^+ channels are known to regulate SC excitability (Molineux *et al.* 2005; Anderson *et al.* 2013; Alexander *et al.* 2019), they do not increase excitability by hyperpolarizing the AP threshold. Furthermore, our previous study demonstrated that other ion channel families typically associated with the regulation of neuronal excitability (delayed rectifier K^+, voltage-dependent Ca^{2+}, and I_h currents) do not contribute to AP threshold hyperpolarization in SCs (Alexander *et al.* 2019).

Cytosolic Ca^{2+} and CaMKII regulate stellate cell excitability via voltage-gated sodium channels

To directly test whether cytosolic Ca^{2+} or CaMKII regulates SC excitability by acting through Na_v channels,

we performed voltage-clamp experiments to record isolated Na^+ membrane currents (Fig. 3). We recorded isolated Na^+ currents using the prepulse activation protocol adapted from Milescu *et al.* (2010) and used in our previous study (Alexander *et al.* 2019).

In control cells, both peak Na_v channel activation and steady-state inactivation relationships shifted in a hyperpolarizing direction following patch breakthrough (Fig. 3*A–C*). The $V_{1/2}$ estimated for Na_v channel peak activation was -32.5 ± 2.9 mV at the beginning of the experiment and -40.2 ± 3.2 mV ($n = 11$) after 25 min of recording corresponding to a hyperpolarizing shift of 7.7 ± 1.7 mV (Fig. 3*B* and *C*). The F-ratio test of the sum of squares between the two Boltzmann fits of the conductance–voltage data at the start and after 25 min yielded a highly significant difference ($F = 40.72$, $P < 0.001$; $n = 11$). Likewise, the $V_{1/2}$ estimated for steady-state Na_v channel inactivation was -49.3 ± 1.3 mV at the start of the experiment and -57.4 ± 2.0 mV ($n = 11$) after 25 min of recording, corresponding to a hyperpolarizing shift of 8.1 ± 1.8 mV (Fig. 3*B* and *D*), whose F-ratio test of Boltzmann fits also yielded a highly significant difference ($F = 277.6$, $P < 0.001$; $n = 11$).

Following treatment with BAPTA and BAPTA-AM, the degree of shift in peak Na_v channel activation was attenuated (Fig. 3*B* and *C*). The F-ratio test of the Boltzmann fits at baseline yielded no significant difference between control and BAPTA internal ($F = 0.82$, $P = 0.45$, $n = 5$ cells) or BAPTA-AM ($F = 2.64$, $P = 0.088$, $n = 5$ cells), demonstrating that the voltage-dependencies of activation between these conditions have the same initial properties (Figs 3*B* and *C* and 4*A*). After 25 min of recording, however, F-ratio tests comparing fits of the conductance–voltage plots yielded significant differences between control and BAPTA internal ($F = 9.27$, $P < 0.001$) or BAPTA-AM ($F = 6.72$, $P = 0.0041$) conditions (Fig. 4*A*). This finding demonstrates that Ca^{2+} chelation significantly attenuates the time-dependent shift in Na_v channel activation. Boltzmann fits comparing Na_v channel activation between control and KN93-treated cells trended towards significance, even with baseline values ($F = 3.03$, $P = 0.063$, $n = 5$ cells) (Fig. 4*B*); therefore, it was not possible to make the same statistical comparison as before. Given this, we compared time-dependent changes in $V_{1/2}$ values ($\Delta V_{1/2}$) between control and KN93 recordings. The $\Delta V_{1/2}$ values were significantly attenuated in the presence of KN93 compared with control cells ($\Delta -4.3 \pm 1.1$ mV for KN93 *vs.* $\Delta -7.7 \pm 1.7$ mV for control; $t = 2.56$, $P = 0.023$) (Fig. 3*C*). Together, these results demonstrate that both cytosolic Ca^{2+} and CaMKII elicit a hyperpolarizing shift in Na_v activation in SCs, the gating parameter most intimately linked to AP threshold (Alexander *et al.* 2019).

Surprisingly, baseline properties of steady-state Na_v channel inactivation were different between control,

BAPTA internal, BAPTA-AM and KN93 conditions (Figs 3D and 4C). The F-ratio test on the Boltzmann fits comparing each condition showed a highly significant difference between all groups at baseline ($F = 277.6$, $P < 0.001$) (Fig. 4C). The $V_{1/2}$ values of both BAPTA internal (-46.1 ± 2.6 mV; $n = 5$) and BAPTA-AM (-43.9 ± 2.5 mV; $n = 5$) were significantly depolarized compared with the control (-49.3 ± 0.7 mV; $n = 11$), whereas the $V_{1/2}$ value measured in the presence of KN93 was significantly hyperpolarized (-54.4 ± 1.9 mV; $n = 5$) (one-way ANOVA, $F_{4, 33} = 14.81$, $P < 0.001$) (Fig. 3D and 4C). Similarly, Boltzmann fits of the Na_v

channel steady-state inactivation relationships between all conditions after 25 min of recording were also significantly different ($F = 109.5$, $P < 0.001$) (Fig. 4C). As before, we therefore compared the $\Delta V_{1/2}$ values between control and all other conditions. While no significant differences were found between control and either BAPTA internal ($\Delta-6.8 \pm 1.8$ mV for BAPTA internal *vs.* $\Delta-8.1 \pm 1.8$ mV for control; Fisher's LSD, $P = 0.28$) or BAPTA-AM ($\Delta-6.8 \pm 0.7$ mV for BAPTA-AM *vs.* $\Delta-8.1 \pm 1.8$ mV for control; Fisher's LSD, $P = 0.28$), the shift in $V_{1/2}$ inactivation was significantly attenuated in the presence of KN93 ($\Delta-4.2 \pm 1.8$ mV
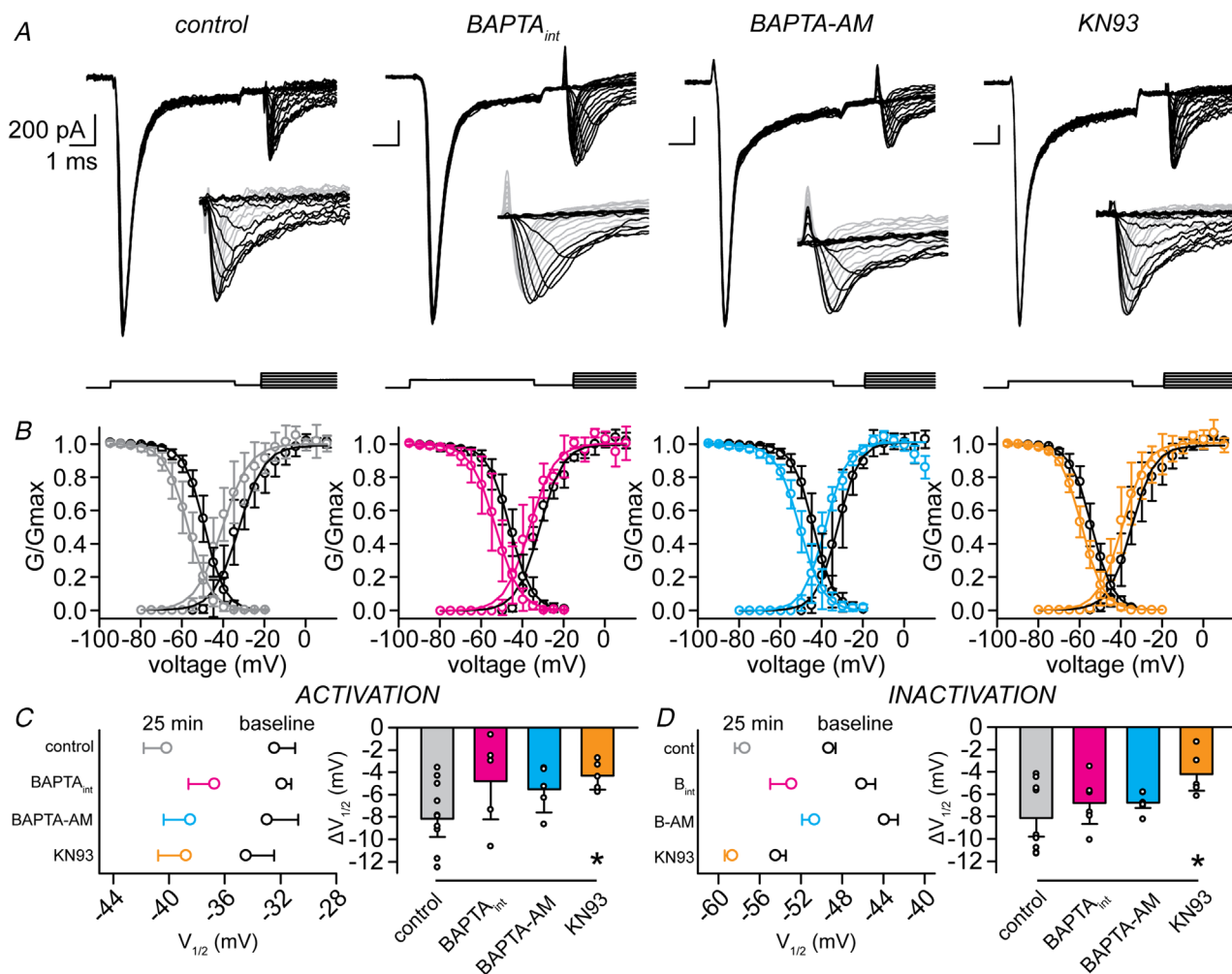

Figure 3. Cytosolic Ca²⁺ and CaMKII regulate shifts in sodium channel-gating properties
A, voltage-clamp traces from example stellate cells (SCs) in response to prepulse activation protocol from each labelled condition. Insets are zoom-ins of I_{Na} peaks used for the calculation of each conductance–voltage relationship. Left: control (patch # 170222p4); centre left: 10 mM BAPTA internal (patch # 190308p2); centre right: 150 μM BAPTA-AM (patch # 190318p4); right: KN93 (patch # 171030p2). *B*, summary voltage-dependence of peak conductance and steady-state inactivation functions for each condition at baseline (black lines) and after 25 min (coloured lines). *C*, (left) mean absolute $V_{1/2}$ activation at baseline (black lines) and 25 min (coloured lines) in each condition. Statistical notation refers to Fisher's LSD *post hoc* test of KN-93 compared with the control condition. (right) Changes in $V_{1/2}$ activation ($\Delta V_{1/2}$) between baseline and after 25 min of recording across all conditions. *D*, same as in (*C*) but for $V_{1/2}$ of steady-state inactivation. Sample sizes for (*B*), (*C*) and (*D*): control, $n = 11$ cells; BAPTA internal, $n = 5$ cells; BAPTA-AM, $n = 5$ cells; KN93, $n = 5$ cells. Data are depicted as means $\pm$ SD. *$P < 0.05$.

for KN93 *vs.* $\Delta -8.1 \pm 1.8$ mV for control; Fisher's LSD, $P = 0.006$) (Fig. 3*D*). These findings demonstrate two important factors regarding the regulation of Na_v channel steady-state inactivation in SCs. First, this gating property is highly constitutively regulated by both cytosolic Ca^{2+} concentration and CaMKII activity, each having opposing effects at baseline. With that said,

our previous modelling work suggests that a shift in steady-state inactivation primarily impacts AP amplitude and frequency as opposed to setting the threshold (Alexander *et al.* 2019), although this observation could reflect a heterogeneity of Na_v channel distribution or subunit type. Second, the time-dependent shift in steady-state inactivation of Na_v channels is largely Ca^{2+}-independent,

Figure 4. I_{Na} conductance–voltage relationship comparisons
A, summary voltage-dependence of peak sodium conductance in control (black; $n = 11$ cells), BAPTA internal (magenta; $n = 5$ cells), and BAPTA-AM (blue; $n = 5$ cells) conditions at baseline (left) and after 25 min of recording (right). Pairwise F-ratio tests were performed on Boltzmann fits of conductance–voltage data between each condition. Text colour refers to corresponding BAPTA condition and control. *B*, same for control and KN93 (orange; $n = 5$ cells) conditions. *C*, same for voltage-dependence of steady-state inactivation data for all pharmacological conditions at baseline (left) and after 25 min (right).
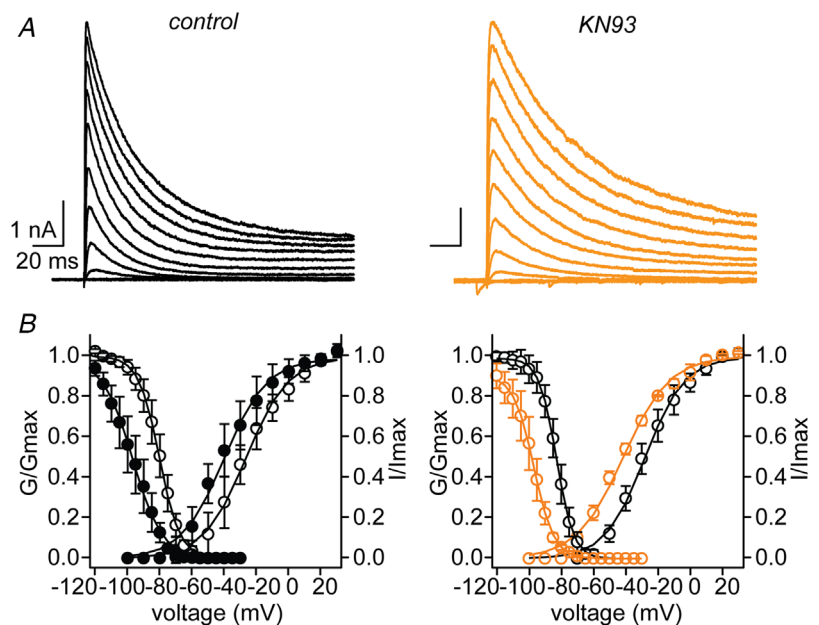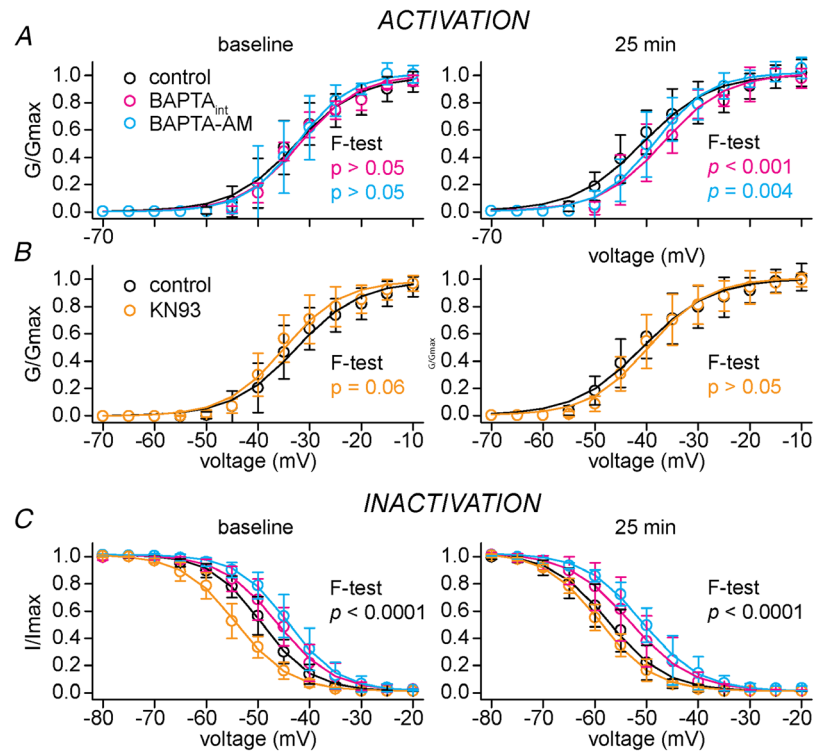

Figure 5. CaMKII activity is not involved in shifts in A-type K^+ channel gating
A, voltage-clamp traces of A-type K^+ current evoked during activation protocols. Left: control (patch # 161024p3); right: KN93 (patch # 161202p1). *B*, superimposed voltage-dependence of activation and steady-state inactivation curves of each pharmacological condition at baseline (open circles) and after 25 min (filled circles or coloured lines). Sample sizes for (*B*): control, $n = 7$ cells; KN93, $n = 5$ cells. Data are depicted as means $\pm$ SD.

and instead depends primarily on CaMKII activation following whole-cell patch clamp. Together, these data give important insight into the regulation of Na_v channels in SCs, both at rest and following establishment of whole-cell recording.

We also examined the effect of inhibiting CaMKII with KN93 on isolated A-type K^+ channels (Fig. 5) since they are known to regulate AP firing rates (Anderson *et al.* 2013). Like Na_v channels, we also observed hyperpolarizing shifts in both the activation and inactivation relationships of isolated A-type K^+ currents following patch breakthrough (Fig. 5*A* and *B*). The $V_{1/2}$ estimated for K^+ channel peak activation was -25.8 ± 4.6 mV at the beginning of the experiment and -39.1 ± 5.0 mV after 25 min of recording, corresponding to a hyperpolarizing shift of 13.3 ± 6.5 mV ($n = 7$) (Fig. 5*B*). Likewise, the $V_{1/2}$ estimated for steady-state K^+ channel inactivation was -80.7 ± 5.4 mV at the beginning of the experiment and -96.5 ± 7.8 mV after 25 min of recording, corresponding to a hyperpolarizing shift of 15.8 ± 2.6 mV ($n = 7$) (Fig. 5*B*). KN93 did not significantly affect the shift in activation ($\Delta -11.8 \pm 3.8$ mV for KN93 *vs.* $\Delta -13.3 \pm 6.5$ mV for control; $t = 0.35$, $P = 0.73$; $n = 5$) or inactivation ($\Delta -15.3 \pm 3.5$ mV for KN93 *vs.* $\Delta -15.8 \pm 2.6$ mV for control; $t = 0.22$, $P = 0.83$; $n = 5$) compared with controls. These findings demonstrate that the attenuation of AP threshold observed by inhibiting CaMKII (Fig. 2) was not due to an effect on A-type K^+ channels.

Dialysis by the internal patch solution does not increase stellate cell excitability

To test whether dialysis by the internal patch solution was responsible for the increase in excitability, we observed cerebellar SC firing rates under conditions that minimized disruption of the membrane integrity and/or the cytoplasmic content. We first performed giga-ohm seal, cell-attached patch recordings and observed unexpectedly that the frequency of spontaneous action currents increased significantly over the course of the next 25 min whether the patch pipettes contained either high K^+ (1.7 ± 0.3-fold change at 25 min; $t = 4.70$, $P = 0.0022$; $n = 8$) or high Na^+ (1.7 ± 0.5-fold change at 25 min; $t = 2.87$, $P = 0.021$; $n = 9$) (Fig. 6*A–C*). Given this, we concluded that perhaps even mechanical perturbations to the plasma membrane might be sufficient to induce changes in excitability. Importantly, the mechanical stress arising from the patch pipette does not directly open extrasynaptic NMDARs in SCs (Clark and Cull-Candy, 2002), which have been shown elsewhere to be mechanosensitive under certain conditions (Paoletti & Ascher, 1994). In keeping with this, the open channel blocker, MK-801 (10 μM) did not prevent the increase in

spontaneous AP firing following tight-seal formation (1.9 ± 0.6-fold change at 25 min; $t = 2.76$, $P = 0.039$; $n = 6$). Furthermore, we repeated the experiments using loose-seal patch recordings of less than 60 MΩ and observed that firing rates were constant throughout the recording period (1.0 ± 0.1-fold change at 15 min; $t = 0.36$, $P = 0.73$; $n = 12$) (Fig. 6*C*). The fact that seal resistance has a time-dependent influence on SC excitability is not entirely surprising as other studies have reported evidence of a mechanosensitive signalling pathway in this cell type (Chavas *et al.* 2004; Alcami *et al.* 2012).

To explore this point further and directly address the role of cytoplasmic washout, current-clamp recordings were performed using the tight-seal, perforated-patch mode to significantly limit dialysis by the internal solution (Fig. 6*D* and *E*). To do this, the antibiotic amphotericin B (300 μg ml^{-1}) was included in the internal solution along with Lucifer Yellow (1 mM) to monitor the integrity of the plasma membrane and exclude ruptured patches from analysis (Fig. 6*D*; see also Kass & Mintz (2006)). Using this approach, SC excitability remained stable over the duration of the recording suggesting that cytoplasmic dialysis may be an important factor contributing to the increase in excitability. For example, the number of APs evoked by a 16 pA step current did not significantly change over a 25 min recording duration (10.2 ± 8.3 at baseline *vs.* 10.6 ± 7.7 at 25 min; $t = 0.43$, $P = 0.69$; $n = 5$) (Fig. 6*E*). In agreement with this, the time-dependent, hyperpolarizing shift in AP threshold observed in whole-cell experiments was also significantly attenuated ($\Delta -2.8 \pm 1.3$ mV for perforated patch *vs.* $\Delta -8.3 \pm 1.1$ mV for control; $t = 6.00$, $P < 0.001$; perforated patch: $n = 5$, control: $n = 11$) (Fig. 6*F*).

However, when the time lag required to obtain a perforated-patch recording was accounted for (>10 min, Fig. 6*G*), we observed a significant delay before the first measurement could be obtained and that the AP threshold was then significantly hyperpolarized (-49.4 ± 3.6 mV for perforated patch *vs.* -39.5 ± 1.8 mV for control; $t = 5.16$, $P < 0.001$) (Fig. 6*F*). Given this significant delay and appreciating that SC excitability increases in tight-seal recordings (Fig. 6*A–C*), we reasoned that the apparent stability we had observed in firing rates with perforated-patch recordings (Fig. 6*E*) corresponded to the fact that the increase in membrane excitability had already reached its maximum level. To test this, the relationship between the baseline AP threshold (ordinate) and time to obtain a first measurement (abscissa) was compared across all patch configuration modes, including the unintentionally ruptured patches (Fig. 6*G*). Consistent with our hypothesis, we observed a significant negative slope between time delay post-seal and baseline threshold (Pearson's $r = -0.70$, $P = 0.002$; $n = 17$) (Fig. 6*G*), demonstrating that the hyperpolarization in the AP

threshold proceeds regardless of configuration, even when the cytoplasm is intact. Given this, all subsequent experiments described in Figs 8 and 9 were performed in the loose-seal, cell-attached configuration.

## NMDA receptors upregulate the intrinsic excitability of stellate cells via Ca^{2+} and CaMKII

Since the activation of postsynaptic NMDARs elevates cytosolic Ca^{2+} and stimulates CaMKII (Malenka & Nicoll, 1999), we performed separate experiments to determine whether the hyperpolarizing shift in Na_v channel gating could be triggered by bath application of NMDA (Fig. 7) and/or the presynaptic release of the neurotransmitter, L-glutamate (L-glu) (Fig. 8). In each case, we recorded spontaneous action currents from SCs using loose-seal, cell-attached recordings which avoids the complications initiated by tight-seal cell-attached and whole-cell recordings, as noted previously (Fig. 6; see also Alcami *et al.* (2012)). We added the $GABA_A$ and AMPA receptor antagonists, bicuculline (10 μM) and

NBQX (10 μM), respectively, to the bath solution to pharmacologically isolate the NMDA receptor response.

In cell-attached mode, SC firing rates remained stable during the first 15 min of recording (5.2 $\pm$ 3.7 Hz at 1 min *vs.* 5.1 $\pm$ 4.1 Hz at 15 min; $t = 0.21$, $P = 0.84$; $n = 7$) (Fig. 7A and C). Subsequent bath application of NMDA (50 μM, 3 min) elicited a reversible increase in firing rates (4.9 $\pm$ 3.7 Hz at baseline *vs.* 21.4 $\pm$ 7.2 Hz during NMDA application; $t = 4.15$, $P = 0.006$; $n = 7$) (Fig. 7A and C) which subsided after agonist washout, reflecting the depolarizing action of NMDA on the resting membrane potential. Interestingly, 30 min after removal of NMDA, firing rates were significantly augmented about fourfold compared with the baseline (3.8 $\pm$ 1.8-fold change at 30 min; $t = 3.00$, $P = 0.024$; $n = 7$) (Fig. 7B and C). The increase in firing rates was completely blocked by either incubating cerebellar slices in BAPTA-AM (150 μM; 1.3 $\pm$ 0.5-fold change at 30 min; $t = 1.23$, $P = 0.29$; $n = 5$) (Fig. 7B and C) or KN93 (5 μM; 1.6 $\pm$ 1.0-fold change at 30 min; $t = 1.20$, $P = 0.30$; $n = 5$) (Fig. 7B and C), demonstrating that NMDAR activation mediates its effects through an

Figure 6. Stellate cell excitability increase is dialysis-independent
A, example traces of spontaneous action currents recorded in tight-seal cell-attached configuration with either high K^+ (left) (patch # 140228p1) or Na^+ internal (right) (patch # 190916p1) at baseline or 25 min later. *B*, plots depicting normalized firing rate at baseline and 25 min after seal formation of individual cells (lines) and summary averages (bars). Paired *t* tests were used to compare these data. *C*, time course plot of summary normalized firing data over multiple cells in each condition (K^+ internal, $n = 8$ cells; Na^+ internal, $n = 9$ cells; + MK-801, $n = 6$ cells; loose-seal, $n = 12$ cells). *D*, example images of intact and unintentionally ruptured perforated-patch configuration of neurons in slice, visualized using Lucifer Yellow. *E*, example current-clamp traces from a stellate cell recorded in whole-cell (patch # 150129p2) or perforated-patch configuration (patch # 180702p1) depicting APs evoked by step currents at baseline and after 25 min. *F*, summary plot of AP threshold over time comparing whole-cell ($n = 12$ cells) to perforated-patch data ($n = 5$ cells). *G*, correlation analysis using Pearson's coefficient demonstrates a significant relationship between time post-seal and AP threshold measured at baseline, regardless of configuration. Graphs depict means $\pm$ SD. *$P < 0.05$, **$P < 0.01$.
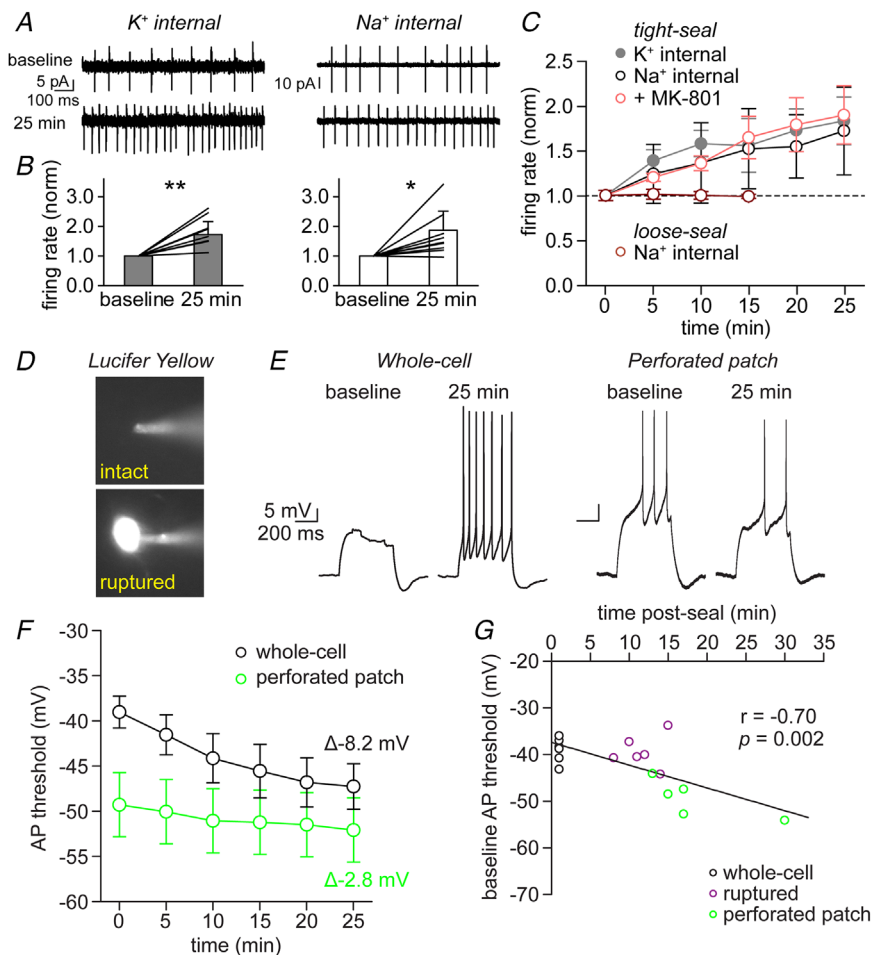
increase in cytosolic Ca^{2+} and activation of CaMKII. Notably, absolute firing rates measured at baseline in BAPTA-AM were significantly increased compared with control tissue (one-way ANOVA, $F_{2,16} = 3.61$, $P = 0.054$; Fisher's LSD, $P = 0.032$) (Fig. 7D), which may reflect the role of Ca^{2+}-activated K^+ channels in regulating basal firing. The fact that basal firing rates were unchanged in the presence of KN93 provides compelling evidence that the NMDA receptor-mediated effects harness the same signalling pathway as that triggered by patch break-through to establish whole-cell recordings (Figs 2 and 3).

To determine whether synaptic release of L-glu could also induce intrinsic plasticity, we used an extracellular electrode to stimulate the PFs of axons from granule cells which represent the primary excitatory afferent input to SCs. Since NMDARs expressed by SCs are located outside the synapse (Carter & Regehr, 2000; Clark & Cull-Candy, 2002), a high frequency stimulation protocol of PFs (six

pulses at 100 Hz, every 5 min for 30 min) was used to promote neurotransmitter spillover. As before, loose-seal, cell-attached recordings were performed in the presence of 10 μM bicuculline, but in the absence of NBQX to ensure that glutamatergic transmission was intact. Under these conditions, SC firing rates remained stable during the trial period of 15 min (2.9 ± 0.6 Hz at 1 min *vs.* $3.0 \pm 0.6 \pm$ at 15 min; $t = 1.02$, $P = 0.35$; $n = 7$ cells) (Fig. 8A and C). Following high frequency stimulation of PFs, the spontaneous firing rates of SCs increased significantly, representing a 2.2 ± 0.7-fold increase over the course of 30 min ($t = 3.10$, $P = 0.021$; $n = 7$) (Fig. 8B and C). Importantly, the increase in firing rates observed following high frequency stimulation of PFs was eliminated in SCs incubated in the NMDA receptor competitive antagonist, D-APV (10 μM; 0.9 ± 0.3-fold change at 30 min; $t = 0.50$, $P = 0.64$; $n = 5$) (Fig. 8B and C). Furthermore, SC firing rates also remained stable
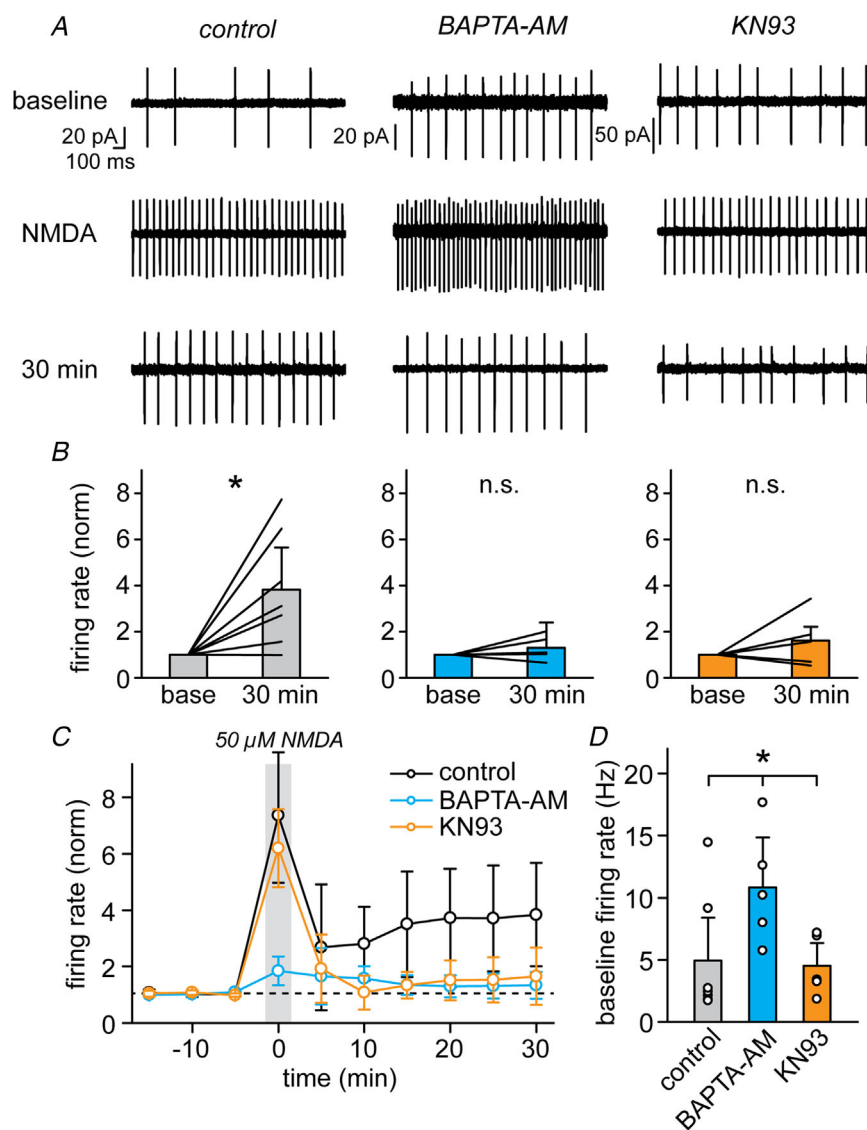

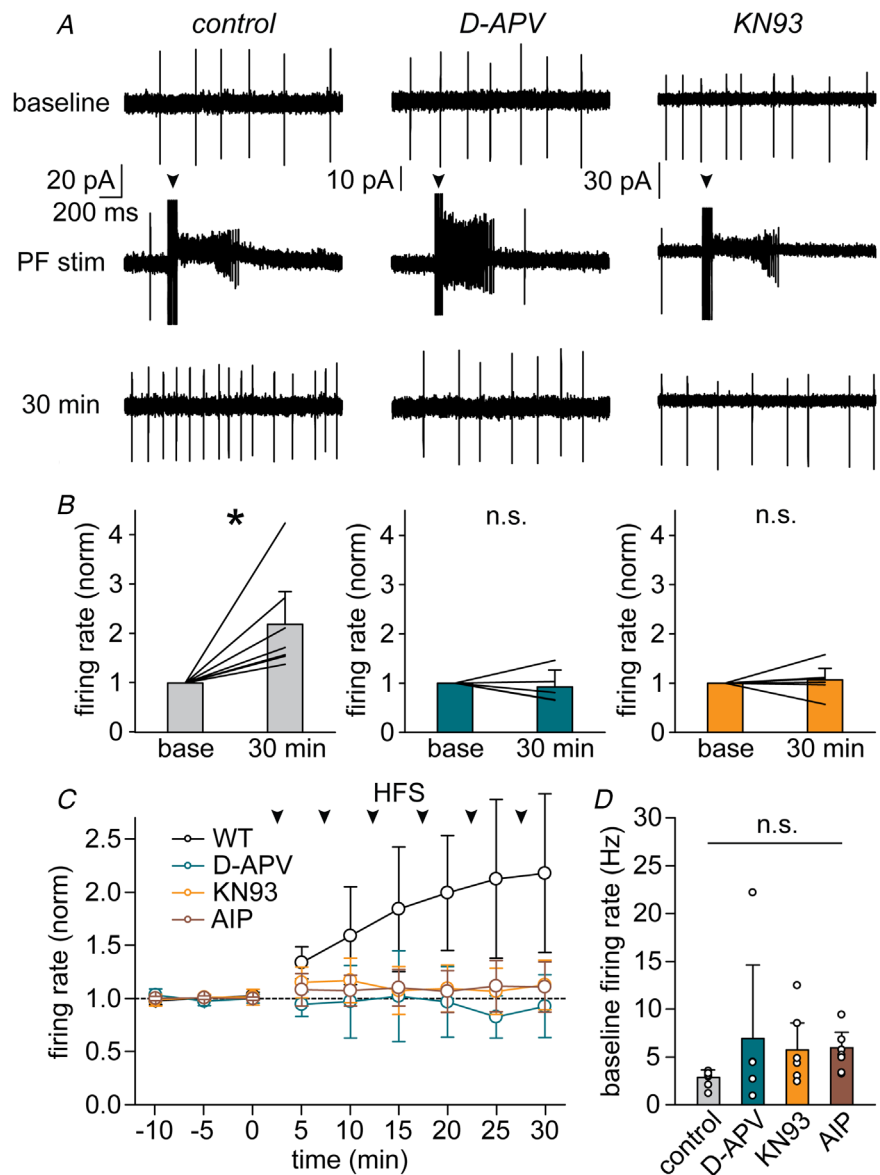**Figure 7. NMDA receptor stimulation induces excitability increase in a Ca^{2+}- and CaMKII-dependent manner**
A, example loose-seal cell-attached recordings from a stellate cell (SC) at baseline, during 3 min bath application of 50 μM NMDA, and 30 min following NMDA washout in normal ACSF (left) (patch # 190411p4), following >1 h incubation in 150 μM BAPTA-AM (centre) (patch # 190416p3), and in the presence of 5 μM KN93 (right) (patch # 190417p4). *B*, plots depicting normalized firing rate at baseline and 30 min after NMDA exposure of individual cells (lines) and summary averages (bars). Using unpaired *t* tests, a significant increase in normalized SC firing was induced by NMDA application in the control condition (grey; $n = 7$ cells) that could be occluded by BAPTA-AM (blue; $n = 5$ cells) or KN93 (orange; $n = 5$ cells). *C*, time course plot of summary normalized firing data over multiple cells in each condition. *D*, absolute firing rate summary data for each pharmacological condition show that cells incubated in BAPTA-AM had significantly increased excitability at baseline based on one-way ANOVA. Graphs depict means $\pm$ SD. *$P < 0.05$.

when CaMKII activity was inhibited using KN93 (5 μM; 1.1 $\pm$ 0.2-fold change at 30 min; $t = 0.58$, $P = 0.57$; $n = 7$) and AIP (1 μM; 1.1 $\pm$ 0.2-fold change at 30 min; $t = 0.89$, $P = 0.40$; $n = 7$) (Fig. 8*B* and *C*). Importantly, none of these pharmacological conditions had any significant impact on baseline firing rates compared with control (one-way ANOVA, $F_{3, 23} = 1.07$, $P = 0.38$) (Fig. 8*D*). Lastly, NMDARs have recently been shown to elevate NO in SCs (Larson *et al.* 2020), and therefore we investigated whether NO could contribute to the induction of intrinsic plasticity. Blocking the activity of nitric oxide synthase (nNOS) with 3-Br-7-Ni (10 μM) still resulted in elevated firing rates at 30 min post-PF stimulation (1.8 $\pm$ 0.8-fold change at 30 min; $t = 2.47$, $P = 0.048$; $n = 8$), demonstrating that NO signalling does not play a significant role. Together, these findings show

that the synaptic release of L-glu using physiologically relevant activation patterns induces intrinsic plasticity in SCs through a NMDA receptor- and CaMKII-dependent signalling pathway.

Discussion

The present study advances our understanding of the neurophysiology of cerebellar SCs in several important ways. First, we show that extrasynaptic NMDARs regulate the intrinsic excitability of SCs through a novel plasticity mechanism. Although not studied here, the increase in AP firing elicited by NMDARs would be expected to augment presynaptic release of GABA and inhibitory LTP on post-synaptic Purkinje cells and other SCs. Second, we establish that the increase in intrinsic excitability is controlled

Figure 8. Parallel fibre stimulation induces excitability increase in a NMDA receptor- and CaMKII-dependent manner
A, example loose-seal cell-attached recordings from a stellate cell (SC) during baseline, 100 Hz parallel fibre (PF) stimulation, and 30 min after stimulation in normal ACSF (left) (patch # 191009p3), in the presence of 10 μM D-APV (centre) (patch # 191101p4), and 5 μM KN93 (right) (patch # 200113p1). *B*, plots depicting normalized firing rate at baseline and 30 min after PF stimulation of individual cells (lines) and summary averages (bars). *C*, time course plot of summary normalized firing data over multiple cells in control (black; $n = 7$ cells), D-APV (dark cyan; $n = 5$ cells), KN93 (orange; $n = 7$ cells) and AIP (brown; $n = 7$ cells) conditions. *D*, baseline spontaneous firing rates over all pharmacological conditions. Graphs depict means $\pm$ SD. *$P < 0.05$ using unpaired t tests and one-way ANOVA.

by both Ca^{2+} and CaMKII which modify the gating behaviour of Na_v channels to lower the threshold for AP initiation. Whether Ca^{2+} and/or CaMKII act directly or indirectly on Na_v channels awaits future investigation. Finally, patch breakthrough, and even excess membrane tension caused by tight-seal patches, bypasses NMDAR stimulation to initiate the identical signalling pathway. These latter findings open the possibility that cerebellar SC excitability may be impacted by mechanical perturbation *in vivo* that include, for example, changes to the extracellular space. It also emphasizes the need in future studies to maintain the membrane integrity of cerebellar SCs if their network properties are to be elucidated.

Not all sources of Ca^{2+} induce intrinsic plasticity of cerebellar stellate cells

Our data show unexpectedly that only Ca^{2+} entering through NMDARs triggers the onset of intrinsic plasticity in SCs of the cerebellum. SCs express Ca^{2+}-permeable AMPARs (Liu & Cull-Candy, 2000) and metabotropic GluRs (mGluRs) (Llano & Marty, 1995), which could, in principle, evoke large transients in cytoplasmic Ca^{2+} to trigger the onset of intrinsic plasticity. However, our experiments with the selective NMDAR competitive antagonist, APV (Fig. 8*A–C*) and MK801 (Alexander & Bowie, unpublished observation) reveal that the onset of intrinsic plasticity is prevented even though signalling by CP-AMPARs and mGluRs is intact. Similarly, these data establish that Ca^{2+} entry through voltage-gated Ca^{2+} channels is incapable of inducing long-lasting changes in SC excitability. During high frequency PF stimulation, SCs undergo significant iGluR-mediated elevations in AP firing rates which presumably would lead to the activation of voltage-gated Ca^{2+} channels and the transport of Ca^{2+} into the cytoplasm. Despite this, high frequency stimulation of PFs in the presence of APV does not induce long-term changes in the excitability of SCs. Consequently, membrane depolarization in itself is not sufficient to induce intrinsic plasticity. Accordingly, we conclude that only Ca^{2+} entering through NMDARs is capable of triggering the onset of intrinsic plasticity in SCs of the cerebellum.

Non-canonical signalling by NMDARs in inhibitory cerebellar stellate cells

There has been a general debate about non-canonical signalling by NMDARs in different neuronal classes including those of the cerebellum (Dore *et al.* 2017; Bouvier *et al.* 2018). In SCs, for example, several studies have argued that NMDARs function primarily from a presynaptic locale where they elevate local Ca^{2+} levels to promote GABA release (Glitsch & Marty, 1999; Duguid

& Smart, 2004; Huang & Bordey, 2004; Liu, 2007; Glitsch, 2008; Lachamp *et al.* 2009). It has also been proposed that the presynaptic release of GABA is stimulated by dendritic NMDARs which elevate local Ca^{2+} levels in the axon of SCs by electrotonic depolarization of voltage-gated Ca^{2+} channels (Christie & Jahr, 2008; Christie *et al.* 2011). Whether CaMKII or other kinases are involved in the effects of dendritic NMDARs on axonal Ca^{2+} channels has not been investigated. However, protein kinase A has been linked to signalling mediated by presynaptic NMDARs (Lachamp *et al.* 2009), making these observations distinct from the present study. Importantly, these studies were all performed using whole-cell patch-clamp recordings which would have overridden the signalling pathway we report between NMDARs and voltage-gated Na_v channels. As a result, our findings identify an additional mechanism by which NMDARs regulate neuronal excitability of SCs to promote inhibitory neurotransmitter release.

Cerebellar SCs express multiple NMDAR subunits that could assemble into distinct dendritic and presynaptic families with different signalling capacities. Genetic deletion and pharmacology experiments have proposed that SCs express tri-heteromeric NMDARs containing the GluN2B and GluN2D receptor subunits that each bind the neurotransmitter, L-glutamate, as well as the GluN1 subunit which binds the co-agonist, glycine (Dubois *et al.* 2016). In addition, recent findings looking at RNAseq data reveal appreciable levels of the GluN3A but not the GluN3B NMDAR receptor subunit in cerebellar molecular layer interneurons (Zeisel *et al.* 2018), which could substitute for either GluN2B and/or GluN2D to form NMDAR tetramers with distinct signalling properties (Perez-Otano *et al.* 2016). In principle, GluN3 and GluN1 subunits could co-assemble as NMDARs (Awobuluyi *et al.* 2007). However, they have yet to be identified in the cerebellum though they have been observed in CA1 neurons of the developing (P8–12) mouse hippocampus (Grand *et al.* 2018). Though studied to a much lesser extent, emerging findings have already established that GluN3-containing NMDARs have functional properties distinct from GluN2-containing NMDARs that include a lower Ca^{2+} permeability and weaker Mg^{2+} channel block (Perez-Otano *et al.* 2016). It is not known whether GluN3-containing NMDARs preferentially couple to specific cytoplasmic kinases; therefore, it remains to be established whether they play any role in regulating the Na_v channels described in the present study.

Regulation of voltage-gated sodium channels by NMDA receptors and CaMKII

Whether the NMDAR signalling described in the present study corresponds to a contribution from dendritic

or presynaptic receptors or a combination of both is still not clear. However, it raises the question of how Na_v channels are regulated. Based on antibody staining, cerebellar SCs express the Na_v channel pore-forming subunits $Na_v1.1$ and $Na_v1.6$ (Kalume *et al.* 2007), although their subcellular distribution is distinct (Lorincz & Nusser, 2008). The $Na_v1.1$ subunit is almost exclusively expressed at the axon initial segment (AIS), whereas $Na_v1.6$ is expressed throughout the axon including the proximal AIS (Lorincz & Nusser, 2008). Given this arrangement, the proximity of $Na_v1.6$ channels may make them more amenable to direct regulation by presynaptic NMDARs than $Na_v1.1$. The dendrites of cerebellar SCs are apparently devoid of Na_v channels (Myoga *et al.* 2009), so if dendritic NMDARs regulate Na_v channels it would require a remote mechanism that signals to the AIS. An attractive possibility is that NMDAR-mediated depolarization in SC dendrites promotes an electrotonic depolarizing spread into axons to open voltage-gated Ca^{2+} channels (Christie & Jahr, 2008). Activated Ca^{2+} channels would then elevate local Ca^{2+} in the axon to stimulate CaMKII and modulate Na_v channel gating. The subcellular distribution of CaMKII in the AIS has not been studied; however, morphological analysis earmarks the AIS as a hub for other signalling proteins, including other ion channel families (Lorincz & Nusser, 2008), enhancing the likelihood that kinases will be present too.

Most of the work on CaMKII has focused on its regulation of the dominant cardiac isoform, $Na_v1.5$, where many potential phosphorylation sites have been identified (Scheuer, 2011). The primary effect of CaMKII is to hyperpolarize $Na_v1.5$ steady-state inactivation (Wagner *et al.* 2006), although there is some conflicting evidence (Aiba *et al.* 2010). Less is known about the effects of CaMKII on neuronal Na_v channels, but it has been shown to regulate channel availability of $Na_v1.2$ (Thompson *et al.* 2017). This observation is relevant to the present study as applying the CaMKII inhibitor, KN93, shifted baseline Na_v channel steady-state inactivation in SCs (cf. Fig. 3). Although $Na_v1.2$ is not thought to contribute to AP firing in SCs (Alexander & Bowie, unpublished observation), others have demonstrated that CaMKII can have regulatory effects on $Na_v1.1$ channels (Li *et al.* 2018). To our knowledge, this is the first demonstration of CaMKII regulation of Nav1.1 and Nav1.6 that causes a hyperpolarizing shift of both voltage-dependence of activation and steady-state inactivation.

CaMKII need not directly phosphorylate Na_v channels to modify neuronal firing rates but it could occur through the many accessory subunits and binding partners that serve to traffic, accumulate, anchor and modify gating (Ahern *et al.* 2016). Fibroblast growth factors, ankyrins, spectrins and β subunits have all been shown to bind to neuronal sodium channels, with many having a role in channel gating. For example, FGF14 acts as a regulator for $Na_v1.1$ and $Na_v1.6$ channel trafficking in cerebellar Purkinje cells, with knockout animals exhibiting reduced Na_v channel currents and dysregulated AP firing (Xiao *et al.* 2013; Bosch *et al.* 2015). In heart and brain tissue, CaMKII requires the presence of a βIV-spectrin complex to confer its regulatory effects on Na_v channels (Hund *et al.* 2010). Furthermore, CaMKII has been demonstrated to work in concert with FGF12 to negatively shift voltage-dependence of activation in $Na_v1.2$ channels, as well as to promote basal current density in HEK 293 cells (Wildburger *et al.* 2015). Whether any of these mechanisms are at play in cerebellar SCs awaits future investigation.

Is stellate cell excitability regulated by a mechanosensitive pathway?

Our data show unexpectedly that changes in the plasma membrane tension induced by the formation of a giga-ohm seal are sufficient to induce a time-dependent increase in SC excitability (Fig. 6*A*–*C*). Repeating the experiments with loose-seal patch recordings circumvents the increase in excitability (Fig. 6*C*), underlining the role that membrane tension plays. Our perforated-patch experiments (Fig. 6*D*–*G*) further reveal that the increase in excitability observed in conventional whole-cell recordings is most likely first triggered by a rupture in membrane tension which elevates cytoplasmic Ca^{2+}-activating CaMKII before promoting gating shifts in Na_v channels (Figs 3 and 4). Other studies have proposed that SCs possess a mechanosensitive mechanism that can induce rises in cytosolic Ca^{2+} (Chavas *et al.* 2004; Alcami *et al.* 2012). Exactly how changes in membrane tension lead to Ca^{2+} transients is not known and we do not address the source of the Ca^{2+} in this study. However, there is a plethora of candidate mechanosensitive ion channels to consider. For example, Piezo2 readily permeates Ca^{2+} (Szczot *et al.* 2017) and is found in cerebellar neuronal somata (Wang & Hamill, 2020). Emerging channel subfamilies like NALCN and TACAN, which are activated and modulated by non-traditional stimuli, like external Ca^{2+} concentration (Chua *et al.* 2020) and high threshold mechanical stimulation (Beaulieu-Laroche *et al.* 2020), respectively, might also play a role. These types of channels, studied mostly in the periphery, might serve uncharacterized purposes in the brain by acting like extracellular pressure sensors, much like some TRP channel isoforms in the hypothalamic osmoregulatory circuit (Ciura & Bourque, 2006; Sharif Naeini *et al.* 2006), which are crucial in detecting changes to the extracellular space with blood flow (McBain *et al.* 1990; Wang & Hamill, 2020). The fact that cerebellar SCs are so sensitive to external pressure/mechanical perturbation could be important to the synchronization of signal processing in

the cerebellar cortex during vigorous activity, analogous to respiration-entrained oscillatory firing in the olfactory cortex and other brain regions (Zelano *et al.* 2016; Herrero *et al.* 2018; Piarulli *et al.* 2018; Perl *et al.* 2019).

Intrinsic plasticity of stellate cells and its role in the cerebellar circuit

Intrinsic plasticity has been observed in other neurons of the cerebellum including neurons of the deep cerebellar nucleus and granule cells (Aizenman & Linden, 2000; Armano *et al.* 2000). In each case, intrinsic plasticity was induced by NMDARs, although the potential role of CaMKII was not examined nor was the ion channel(s) responsible for the enhancement in membrane excitability identified (Aizenman & Linden, 2000; Armano *et al.* 2000). In fact, intrinsic plasticity via Na_v channel modulation, as reported in the present study, is relatively rare, having been observed only in the prefrontal cortex (Maurice *et al.* 2001; Carr *et al.* 2002; Carr *et al.* 2003) and in the CA1 region of the hippocampus (Xu *et al.* 2005). With the exception of CA1 hippocampal pyramidal cells (Xu *et al.* 2005), all other mechanisms that modify Na_v channel gating have not implicated NMDARs, but instead demonstrated the role of G-protein coupled receptors activated by serotonin or dopamine (Maurice *et al.* 2001; Carr *et al.* 2002, 2003). The increase in intrinsic excitability reported in the hippocampus was due to NMDAR activation and mediated by cytosolic Ca^{2+} and CaMKII which together lowered the AP threshold by shifting Na_v channel activation and inactivation (Xu *et al.* 2005). A potentially important distinction with the present study, however, is that the authors concluded that CaMKII acts locally on Na_v channels in the dendrites of CA1 hippocampal neurons and not remotely on axonal Na_v channels.

Long-term changes in the functionality of Na_v channel gating in SCs may serve several roles. Like basket cells, SCs exhibit a short membrane time-constant and rapid spike initiation (Clark & Cull-Candy, 2002; Jorntell & Ekerot, 2003) that makes them ideal for providing fast and precise spike output to exert feedforward inhibition on Purkinje cells and other molecular layer interneurons. Activity in both stellate and basket cells has been associated with vestibulo-oculomotor reflex gain (Wulff *et al.* 2009), oromotor rhythm tuning (Astorga *et al.* 2017; Gaffield & Christie, 2017), and shaping cutaneous receptive fields *in vivo* (Jorntell & Ekerot, 2003). More recently, it has been shown that activity in both neurons directly controls the plasticity valence of PF EPSPs on Purkinje cells, which has a direct impact on motor learning (Rowan *et al.* 2018). Whether NMDAR-mediated regulation of Na_v channels plays a role in any of these processes or behaviours awaits future investigation.

References

Ahern CA, Payandeh J, Bosmans F & Chanda B (2016). The hitchhiker's guide to the voltage-gated sodium channel galaxy. *J Gen Physiol* **147**, 1–24.

Aiba T, Hesketh GG, Liu T, Carlisle R, Villa-Abrille MC, O'Rourke B, Akar FG & Tomaselli GF (2010). Na+ channel regulation by Ca2+/calmodulin and Ca2+/ calmodulin-dependent protein kinase II in guinea-pig ventricular myocytes. *Cardiovasc Res* **85**, 454–463.

Aizenman CD & Linden DJ (2000). Rapid, synaptically driven increases in the intrinsic excitability of cerebellar deep nuclear neurons. *Nat Neurosci* **3**, 109–111.

Alcami P, Franconville R, Llano I & Marty A (2012). Measuring the firing rate of high-resistance neurons with cell-attached recording. *J Neurosci* **32**, 3118–3130.

Alexander RPD, Mitry J, Sareen V, Khadra A & Bowie D (2019). Cerebellar stellate cell excitability is coordinated by shifts in the gating behavior of voltage-gated Na(+) and A-type K(+) channels. *eNeuro* **6**.

Anderson D, Engbers JD, Heath NC, Bartoletti TM, Mehaffey WH, Zamponi GW & Turner RW (2013). The Cav3-Kv4 complex acts as a calcium sensor to maintain inhibitory charge transfer during extracellular calcium fluctuations. *J Neurosci* **33**, 7811–7824.

Armano S, Rossi P, Taglietti V & D'Angelo E (2000). Long-term potentiation of intrinsic excitability at the mossy fiber-granule cell synapse of rat cerebellum. *J Neurosci* **20**, 5208–5216.

Astorga G, Li D, Therreau L, Kassa M, Marty A & Llano I (2017). Concerted interneuron activity in the cerebellar molecular layer during rhythmic oromotor behaviors. *J Neurosci* **37**, 11455–11468.

Awobuluyi M, Yang J, Ye Y, Chatterton JE, Godzik A, Lipton SA & Zhang D (2007). Subunit-specific roles of glycine-binding domains in activation of NR1/NR3 N-methyl-D-aspartate receptors. *Mol Pharmacol* **71**, 112–122.

Beaulieu-Laroche L, Christin M, Donoghue A, Agosti F, Yousefpour N, Petitjean H, Davidova A, Stanton C, Khan U, Dietz C, Faure E, Fatima T, Macpherson A, Mouchbahani-Constance S, Bisson DG, Haglund L, Ouellet JA, Stone LS, Samson J, Smith M-J, Ask K, Ribeiro-da-Silva A, Blunck R, Poole K, Bourinet E & Sharif-Naeini R (2020). TACAN is an ion channel involved in sensing mechanical pain. *Cell* **180**, 956–967 e917.

Bers DM, Patton CW & Nuccitelli R (2010). A practical guide to the preparation of Ca(2+) buffers. *Methods Cell Biol* **99**, 1–26.

Bosch MK, Carrasquillo Y, Ransdell JL, Kanakamedala A, Ornitz DM & Nerbonne JM (2015). Intracellular FGF14 (iFGF14) Is Required for Spontaneous and Evoked Firing in Cerebellar Purkinje Neurons and for Motor Coordination and Balance. *J Neurosci* **35**, 6752–6769.

Bouhours B, Trigo FF & Marty A (2011). Somatic depolarization enhances GABA release in cerebellar inter-neurons via a calcium/protein kinase C pathway. *J Neurosci* **31**, 5804–5815.

Bouvier G, Larsen RS, Rodriguez-Moreno A, Paulsen O & Sjostrom PJ (2018). Towards resolving the presynaptic NMDA receptor debate. *Curr Opin Neurobiol* **51**, 1–7.

Carr DB, Cooper DC, Ulrich SL, Spruston N & Surmeier DJ (2002). Serotonin receptor activation inhibits sodium current and dendritic excitability in prefrontal cortex via a protein kinase C-dependent mechanism. *J Neurosci* **22**, 6846–6855.

Carr DB, Day M, Cantrell AR, Held J, Scheuer T, Catterall WA & Surmeier DJ (2003). Transmitter modulation of slow, activity-dependent alterations in sodium channel availability endows neurons with a novel form of cellular plasticity. *Neuron* **39**, 793–806.

Carter AG & Regehr WG (2000). Prolonged synaptic currents and glutamate spillover at the parallel fiber to stellate cell synapse. *J Neurosci* **20**, 4423–4434.

Chavas J, Forero ME, Collin T, Llano I & Marty A (2004). Osmotic tension as a possible link between GABA(A) receptor activation and intracellular calcium elevation. *Neuron* **44**, 701–713.

Christie JM & Jahr CE (2008). Dendritic NMDA receptors activate axonal calcium channels. *Neuron* **60**, 298–307.

Christie JM, Chiu DN & Jahr CE (2011). Ca(2+)-dependent enhancement of release by subthreshold somatic depolarization. *Nat Neurosci* **14**, 62–68.

Chua HC, Wulf M, Weidling C, Rasmussen LP & Pless SA (2020). The NALCN channel complex is voltage sensitive and directly modulated by extracellular calcium. *Sci Adv* **6**, eaaz3154.

Ciura S & Bourque CW (2006). Transient receptor potential vanilloid 1 is required for intrinsic osmoreception in organum vasculosum lamina terminalis neurons and for normal thirst responses to systemic hyperosmolality. *J Neurosci* **26**, 9069–9075.

Clark BA & Cull-Candy SG (2002). Activity-dependent recruitment of extrasynaptic NMDA receptor activation at an AMPA receptor-only synapse. *J Neurosci* **22**, 4428–4436.

Coddington LT, Rudolph S, Vande Lune P, Overstreet-Wadiche L & Wadiche JI (2013). Spillover-mediated feedforward inhibition functionally segregates interneuron activity. *Neuron* **78**, 1050–1062.

Constantine-Paton M, Cline HT & Debski E (1990). Patterned activity, synaptic convergence, and the NMDA receptor in developing visual pathways. *Annu Rev Neurosci* **13**, 129–154.

De Koninck P & Schulman H (1998). Sensitivity of CaM kinase II to the frequency of Ca2+ oscillations. *Science* **279**, 227–230.

Dingledine R, Borges K, Bowie D & Traynelis SF (1999). The glutamate receptor ion channels. *Pharmacol Rev* **51**, 7–61.

Dore K, Stein IS, Brock JA, Castillo PE, Zito K & Sjostrom PJ (2017). Unconventional NMDA Receptor Signaling. *J Neurosci* **37**, 10800–10807.

Dubois CJ, Lachamp PM, Sun L, Mishina M & Liu SJ (2016). Presynaptic GluN2D receptors detect glutamate spillover and regulate cerebellar GABA release. *J Neurophysiol* **115**, 271–285.

Duguid IC & Smart TG (2004). Retrograde activation of presynaptic NMDA receptors enhances GABA release at cerebellar interneuron-Purkinje cell synapses. *Nat Neurosci* **7**, 525–533.

Gaffield MA & Christie JM (2017). Movement Rate Is Encoded and Influenced by Widespread, Coherent Activity of Cerebellar Molecular Layer Interneurons. *J Neurosci* **37**, 4751–4765.

Gall D, Roussel C, Susa I, D'Angelo E, Rossi P, Bearzatto B, Galas MC, Blum D, Schurmans S & Schiffmann SN (2003). Altered neuronal excitability in cerebellar granule cells of mice lacking calretinin. *J Neurosci* **23**, 9320–9327.

Glitsch M & Marty A (1999). Presynaptic effects of NMDA in cerebellar Purkinje cells and interneurons. *J Neurosci* **19**, 511–519.

Glitsch MD (2008). Calcium influx through N-methyl-D-aspartate receptors triggers GABA release at interneuron-Purkinje cell synapse in rat cerebellum. *Neuroscience* **151**, 403–409.

Grand T, Abi Gerges S, David M, Diana MA & Paoletti P (2018). Unmasking GluN1/GluN3A excitatory glycine NMDA receptors. *Nat Commun* **9**, 4769.

Hansen KB, Yi F, Perszyk RE, Furukawa H, Wollmuth LP, Gibb AJ & Traynelis SF (2018). Structure, function, and allosteric modulation of NMDA receptors. *J Gen Physiol* **150**, 1081–1105.

Hardingham GE & Bading H (2010). Synaptic versus extrasynaptic NMDA receptor signalling: implications for neurodegenerative disorders. *Nat Rev Neurosci* **11**, 682–696.

Herrero JL, Khuvis S, Yeagle E, Cerf M & Mehta AD (2018). Breathing above the brain stem: volitional control and attentional modulation in humans. *J Neurophysiol* **119**, 145–159.

Herring BE & Nicoll RA (2016). Long-Term Potentiation: From CaMKII to AMPA Receptor Trafficking. *Annu Rev Physiol* **78**, 351–365.

Huang H & Bordey A (2004). Glial glutamate transporters limit spillover activation of presynaptic NMDA receptors and influence synaptic inhibition of Purkinje neurons. *J Neurosci* **24**, 5659–5669.

Huettner JE (2015). Glutamate receptor pores. *J Physiol* **593**, 49–59.

Hund TJ, Koval OM, Li J, Wright PJ, Qian L, Snyder JS, Gudmundsson H, Kline CF, Davidson NP, Cardona N, Rasband MN, Anderson ME & Mohler PJ (2010). A beta(IV)-spectrin/CaMKII signaling complex is essential for membrane excitability in mice. *J Clin Invest* **120**, 3508–3519.

Jorntell H & Ekerot CF (2003). Receptive field plasticity profoundly alters the cutaneous parallel fiber synaptic input to cerebellar interneurons in vivo. *J Neurosci* **23**, 9620–9631.

Jorntell H & Ekerot CF (2006). Properties of somatosensory synaptic integration in cerebellar granule cells in vivo. *J Neurosci* **26**, 11786–11797.

Kalume F, Yu FH, Westenbroek RE, Scheuer T & Catterall WA (2007). Reduced sodium current in Purkinje neurons from Nav1.1 mutant mice: implications for ataxia in severe myoclonic epilepsy in infancy. *J Neurosci* **27**, 11065–11074.

Kass JI & Mintz IM (2006). Silent plateau potentials, rhythmic bursts, and pacemaker firing: three patterns of activity that coexist in quadristable subthalamic neurons. *Proc Natl Acad Sci U S A* **103**, 183–188.

Lachamp PM, Liu Y & Liu SJ (2009). Glutamatergic modulation of cerebellar interneuron activity is mediated by an enhancement of GABA release and requires protein kinase A/RIM1alpha signaling. *J Neurosci* **29**, 381–392.

Larson EA, Accardi MV, Wang Y, D'Antoni M, Karimi B, Siddiqui T & Bowie D (2020). Nitric oxide signaling strengthens inhibitory synapses of cerebellar molecular layer interneurons through a GABARAP-dependent mechanism. *J Neurosci* **40**, 3348–3359.

Levitan IB (1994). Modulation of ion channels by protein phosphorylation and dephosphorylation. *Annu Rev Physiol* **56**, 193–212.

Li J, Yu Z, Xu J, Feng R, Gao Q, Boczek T, Liu J, Li Z, Wang Q, Lei M, Gong J, Hu H, Minobe E, Ji HL, Kameyama M & Guo F (2018). The Effect of Ca(2+), Lobe-Specificity, and CaMKII on CaM Binding to NaV1.1. *Int J Mol Sci* **19**.

Liu SJ (2007). Biphasic modulation of GABA release from stellate cells by glutamatergic receptor subtypes. *J Neurophysiol* **98**, 550–556.

Liu SJ & Lachamp P (2006). The activation of excitatory glutamate receptors evokes a long-lasting increase in the release of GABA from cerebellar stellate cells. *J Neurosci* **26**, 9332–9339.

Liu SJ, Lachamp P, Liu Y, Savtchouk I & Sun L (2008). Long-term synaptic plasticity in cerebellar stellate cells. *Cerebellum* **7**, 559–562.

Liu SQ & Cull-Candy SG (2000). Synaptic activity at calcium-permeable AMPA receptors induces a switch in receptor subtype. *Nature* **405**, 454–458.

Llano I & Marty A (1995). Presynaptic metabotropic glutamatergic regulation of inhibitory synapses in rat cerebellar slices. *J Physiol* **486**:163–176.

Lorincz A & Nusser Z (2008). Cell-type-dependent molecular composition of the axon initial segment. *J Neurosci* **28**, 14329–14340.

Madison DV, Malenka RC & Nicoll RA (1991). Mechanisms underlying long-term potentiation of synaptic transmission. *Annu Rev Neurosci* **14**, 379–397.

Malenka RC & Nicoll RA (1999). Long-term potentiation–a decade of progress? *Science* **285**, 1870–1874.

Maurice N, Tkatch T, Meisler M, Sprunger LK & Surmeier DJ (2001). D1/D5 dopamine receptor activation differentially modulates rapidly inactivating and persistent sodium currents in prefrontal cortex pyramidal neurons. *J Neurosci* **21**, 2268–2277.

McBain CJ, Traynelis SF & Dingledine R (1990). Regional variation of extracellular space in the hippocampus. *Science* **249**, 674–677.

Milescu LS, Bean BP & Smith JC (2010). Isolation of somatic Na+ currents by selective inactivation of axonal channels with a voltage prepulse. *J Neurosci* **30**, 7740–7748.

Molineux ML, Fernandez FR, Mehaffey WH & Turner RW (2005). A-type and T-type currents interact to produce a novel spike latency-voltage relationship in cerebellar stellate cells. *J Neurosci* **25**, 10863–10873.

Myers SJ, Yuan H, Kang JQ, Tan FCK, Traynelis SF & Low CM (2019). Distinct roles of GRIN2A and GRIN2B variants in neurological conditions. *F1000Res* **8**.

Myoga MH, Beierlein M & Regehr WG (2009). Somatic spikes regulate dendritic signaling in small neurons in the absence of backpropagating action potentials. *J Neurosci* **29**, 7803–7814.

Paoletti P & Ascher P (1994). Mechanosensitivity of NMDA receptors in cultured mouse central neurons. *Neuron* **13**, 645–655.

Paoletti P, Bellone C & Zhou Q (2013). NMDA receptor subunit diversity: impact on receptor properties, synaptic plasticity and disease. *Nat Rev Neurosci* **14**, 383–400.

Perez-Otano I, Larsen RS & Wesseling JF (2016). Emerging roles of GluN3-containing NMDA receptors in the CNS. *Nat Rev Neurosci* **17**, 623–635.

Perl O, Ravia A, Rubinson M, Eisen A, Soroka T, Mor N, Secundo L & Sobel N (2019). Human non-olfactory cognition phase-locked with inhalation. *Nat Hum Behav* **3**, 501–512.

Piarulli A, Zaccaro A, Laurino M, Menicucci D, De Vito A, Bruschini L, Berrettini S, Bergamasco M, Laureys S & Gemignani A (2018). Ultra-slow mechanical stimulation of olfactory epithelium modulates consciousness by slowing cerebral rhythms in humans. *Sci Rep* **8**, 6581.

Rancz EA, Ishikawa T, Duguid I, Chadderton P, Mahon S & Hausser M (2007). High-fidelity transmission of sensory information by single cerebellar mossy fibre boutons. *Nature* **450**, 1245–1248.

Rowan MJM, Bonnan A, Zhang K, Amat SB, Kikuchi C, Taniguchi H, Augustine GJ & Christie JM (2018). Graded Control of Climbing-Fiber-Mediated Plasticity and Learning by Inhibition in the Cerebellum. *Neuron* **99**, 999–1015 e1016.

Saviane C & Silver RA (2006). Fast vesicle reloading and a large pool sustain high bandwidth transmission at a central synapse. *Nature* **439**, 983–987.

Scheuer T (2011). Regulation of sodium channel activity by phosphorylation. *Semin Cell Dev Biol* **22**, 160–165.

Sharif Naeini R, Witty MF, Seguela P & Bourque CW (2006). An N-terminal variant of Trpv1 channel is required for osmosensory transduction. *Nat Neurosci* **9**, 93–98.

Szapiro G & Barbour B (2007). Multiple climbing fibers signal to molecular layer interneurons exclusively via glutamate spillover. *Nat Neurosci* **10**, 735–742.

Szczot M, Pogorzala LA, Solinski HJ, Young L, Yee P, Le Pichon CE, Chesler AT & Hoon MA (2017). Cell-Type-Specific Splicing of Piezo2 Regulates Mechanotransduction. *Cell Rep* **21**, 2760–2771.

Thompson CH, Hawkins NA, Kearney JA & George AL, Jr (2017). CaMKII modulates sodium current in neurons from epileptic Scn2a mutant mice. *Proc Natl Acad Sci U S A* **114**, 1696–1701.

Traynelis SF, Wollmuth LP, McBain CJ, Menniti FS, Vance KM, Ogden KK, Hansen KB, Yuan H, Myers SJ & Dingledine R (2010). Glutamate receptor ion channels: structure, regulation, and function. *Pharmacol Rev* **62**, 405–496.

Wagner S, Dybkova N, Rasenack EC, Jacobshagen C, Fabritz L, Kirchhof P, Maier SK, Zhang T, Hasenfuss G, Brown JH, Bers DM & Maier LS (2006). Ca2+/calmodulin-dependent protein kinase II regulates cardiac Na+ channels. *J Clin Invest* **116**, 3127–3138.

Wang J & Hamill OP (2020). Piezo2, a pressure sensitive channel is expressed in select neurons of the mouse brain: a putative mechanism for synchronizing neural networks by transducing intracranial pressure pulses. *bioRxiv* DOI: 10.1101/2020.03.24.006452 .

Wildburger NC, Ali SR, Hsu WC, Shavkunov AS, Nenov MN, Lichti CF, LeDuc RD, Mostovenko E, Panova-Elektronova NI, Emmett MR, Nilsson CL & Laezza F (2015). Quantitative proteomics reveals protein-protein interactions with fibroblast growth factor 12 as a component of the voltage-gated sodium channel 1.2 (nav1.2) macromolecular complex in Mammalian brain. *Mol Cell Proteomics* **14**, 1288–1300.

Wulff P, Schonewille M, Renzi M, Viltono L, Sassoe-Pognetto M, Badura A, Gao Z, Hoebeek FE, van Dorp S, Wisden W, Farrant M & De Zeeuw CI (2009). Synaptic inhibition of Purkinje cells mediates consolidation of vestibulo-cerebellar motor learning. *Nat Neurosci* **12**, 1042–1049.

Xiao M, Bosch MK, Nerbonne JM & Ornitz DM (2013). FGF14 localization and organization of the axon initial segment. *Mol Cell Neurosci* **56**, 393–403.

Xu J, Kang N, Jiang L, Nedergaard M & Kang J (2005). Activity-dependent long-term potentiation of intrinsic excitability in hippocampal CA1 pyramidal neurons. *J Neurosci* **25**, 1750–1760.

Zeisel A, Hochgerner H, Lonnerberg P, Johnsson A, Memic F, van der Zwan J, Haring M, Braun E, Borm LE, La Manno G, Codeluppi S, Furlan A, Lee K, Skene N, Harris KD, Hjerling-Leffler J, Arenas E, Ernfors P, Marklund U & Linnarsson S (2018). Molecular architecture of the mouse nervous system. *Cell* **174**, 999–1014 e1022.

Zelano C, Jiang H, Zhou G, Arora N, Schuele S, Rosenow J & Gottfried JA (2016). Nasal respiration entrains human limbic oscillations and modulates cognitive function. *J Neurosci* **36**, 12448–12467.

Additional information

Data availability statement

All relevant data are available from the authors upon reasonable request.

Supporting information

Additional supporting information may be found online in the Supporting Information section at the end of the article.

Statistical Summary Document